Ore Geology Reviews 101 (2018) 532–555

Contents lists available at ScienceDirect

Ore Geology Reviews

journal homepage: www.elsevier.com/locate/oregeorev

3D reconstruction of volcanic and ore-forming environments of a giant VMS system: A case study from the Kidd Creek Mine, Canada

Y.M. DeWolfe[a,b,*], H.L. Gibson[b], D. Richardson[c,d]

[a] Department of Earth and Environmental Sciences, Mount Royal University, 4825 Mount Royal Gate SW, Calgary, AB T3E 6K6, Canada
[b] Mineral Exploration Research Centre, Department of Earth Sciences, Laurentian University, 933 Ramsey Lake Road, Sudbury, ON P3E 6C7, Canada
[c] Kidd Operations, 11335 Highway 655 North, Timmins, ON P4N 7K1, Canada
[d] Sudbury Integrated Nickel operations - A Glencore Company, 6 Edison Road, Falconbridge, ON P0M 1S0, Canada

ARTICLE INFO

Keywords:
Volcanogenic massive sulfide
Hydrothermal alteration
Subaqueous volcanism
North Rhyolite
Synvolcanic structures
3D volcanic reconstruction

ABSTRACT

The Archean North Rhyolite is a bimodal suite of rocks located directly northwest of, but structurally separate from, the Kidd Creek volcanogenic massive sulfide deposit, which has produced 140.4 million tonnes of ore grading 2.29 wt% Cu, 6.15 wt% Zn, 0.22% Pb and 86.2 g/t Ag. The stratigraphy of the North Rhyolite is identical to that of the Kidd Creek mine consisting, from oldest to youngest, of ultramafic flows, aphyric rhyolite, quartz porphyritic rhyolite, and basalt flows, divisible into a "low TiO_2" basalt unit (< 1.55 wt%) and a "high TiO_2" basalt unit (> 1.55 wt%), with minor interflow graphitic argillites.

The North Rhyolite is interpreted to be the folded continuation of the Kidd Creek mine stratigraphy. Similar alteration patterns in the North Rhyolite and the Kidd Creek mine stratigraphy, as well as significant copper and zinc values within the thickest portions of rhyolite domes and ridges of the North Rhyolite, suggests the potential for economically significant mineralization within the North Rhyolite stratigraphy. Correlation between alteration, mineralization and the rhyolite domes and ridges demonstrate the volcanic structures through which the rhyolite was extruded also acted as hydrothermal fluid pathways and were controlling structures in ore formation.

A 3D volcanic reconstruction, showing the paleo-seafloor at the time of ore-formation, illustrates that the rhyolite flows of the North Rhyolite were emplaced into the same subsidence structure as the strata of the Kidd Creek mine area. This 3D model, generated by translating complex geological data acquired through core logging and underground mapping indicates the volcanic setting of, and ore-forming environment at, Kidd Creek is much larger than previously thought and provides new spatial data that can be used in exploration targeting.

1. Introduction

Volcanogenic massive sulfide (VMS) deposits are an important source of base metals worldwide (e.g., Cu, Zn, Pb). VMS deposits are common in Archean host rocks, and much has been published on the volcanic settings of these deposits, especially those in the Abitibi greenstone Belt of Canada (e.g., Bleeker, 1999; Gibson et al., 1999; Gibson and Galley, 2007; Hudak et al., 2003; Monecke et al., 2008; Rogers et al., 2014; Monecke et al., 2017; Debreil et al., 2018). Continuing to improve our understanding of how volcanic processes and structures related to VMS formation in the Archean, especially those of the economically-important Abitibi greenstone belt, which has produced over 810 Mt of Cu-Zn-Pb (Mercier-Langevin et al., 2011), remains an important objective in the overall understanding of VMS formation. Bi-modal Archean volcanic successions are of particular importance given they host numerous deposits including the 54 Mt Horne (Noranda) and the 140 Mt Kidd Creek VMS orebodies (Bleeker, 1999; Gibson et al., 1999; McNicoll et al., 2014). Detailed documentation of volcanic lithofacies, combined with high precision lithogeochemistry and structural analysis can be used can be used as mappable spatial proxies in targeting mineral deposits and are crucial in locating VMS deposits. This modelling of geological complexities, such as synvolcanic structures defined through detailed lithofacies analysis, can then be used for an improved understanding of volcanic processes, how these impact ore-formation, and consequently in targeting mineral deposits. Here, we present new stratigraphic and lithogeochemical data of the volcanic rocks hosting the Kidd Creek VMS deposit, creating a 3D reconstruction of the volcanic and ore-forming environment at Kidd Creek, in order to better understand the structural and volcanic controls on the largest Archean VMS in the world.

* Department of Earth and Environmental Sciences, Mount Royal University, 4825 Mount Royal Gate SW, Calgary, AB T3E 6K6, Canada
E-mail address: mdewolfe@mtroyal.ca (Y.M. DeWolfe).

https://doi.org/10.1016/j.oregeorev.2018.07.008
Received 14 April 2018; Received in revised form 5 July 2018; Accepted 13 July 2018
Available online 13 August 2018
0169-1368/

A succession of volcanic rocks collectively known as the North Rhyolite (NR) is located directly northwest of, but structurally separate from, the giant Kidd Creek Cu-Zn-Ag deposit and it has been suggested to be the lateral extension of the Kidd Creek mine stratigraphy (Hannington et al., 1999a). If true, this means it is an integral part of the volcanic, subsidence and hydrothermal history that characterized the ore-forming environment at Kidd Creek. Given that the NR is less altered than the Kidd mine stratigraphy it provides a unique opportunity to understand the larger volcanic environment in which the Kidd Creek deposit formed including processes that led to ore formation. Reconstructing the volcanic environment of the NR is paramount not only in understanding controls on ore-formation at Kidd Creek, but facilitates the modelling of geological complexities of VMS deposits, thereby providing a useful exploration targeting tool.

In this study we use spatial data analysis of geological complexities, from underground and drill core data, including detailed litho-geochemistry, to create a 3D model that helps us better understand VMS ore-forming processes. We demonstrate how synvolcanic structures critical in focusing hydrothermal fluids responsible fore ore-formation can be translated (even in polydeformed terranes) into mappable spatial proxies that can be used in mineral exploration targeting.

Accordingly this study presents: (1) a stratigraphic subdivision of the NR that reflects the volcanic history of these rocks and provides a basis for comparison with the structurally separate Kidd mine stratigraphy; (2) detailed descriptions of lithofacies and alteration within the NR that clearly extend the area of rhyolite volcanism and associated hydrothermal alteration from the Kidd mine area to the NR; and (3) a 3D model of the volcanic and hydrothermal setting of an Archean flow-dome complex that illustrates how volcanic structures not only controlled rhyolite distribution, but also, through later reactivation, controlled hydrothermal discharge and associated VMS mineralization.

2. Regional setting

The Kidd Creek deposit is the largest Archean VMS deposit in production and is located 24 km north of Timmins, within the of the Abitibi greenstone belt (2750 to 2650 Ma) of the Superior province (Fig. 1). With approximately 80% of the known Archean VMS tonnage in the world, the Superior craton is by far the most well-endowed (Fyon et al., 1991; Mercier-Langevin et al., 2014). The Superior craton is divided into east-west trending granite-greenstone subprovinces and metasedimentary subprovinces that are bound by the Trans-Hudson orogeny to the west, and the Grenville province to the east. The granite-greenstone subprovinces have been variously described as successive lateral accretions of volcano-plutonic arcs, ocean islands, oceanic plateaus, and rift-related assemblages (e.g., Langford and Morin, 1976; Percival and Card, 1985; Ludden and Hubert, 1986; Ludden et al., 1986; Card, 1990; Jackson and Sutcliffe, 1990; Williams, 1990; Corfu, 1993; Heather et al., 1995; Jackson and Cruden, 1995; Ayers et al., 2002; Thurston et al., 2008).

The Abitibi Subprovince (94 000 km^2) is the largest greenstone belt within the Superior province and it contains some of the most important gold and base metal mining camps in Canada (Hannington et al., 1999a; Gibson and Galley, 2007; Mercier-Langevin et al., 2007; Dubé et al., 2007; Bateman et al., 2008; Ispolatov et al., 2008; Debreil et al., 2018). The Timmins region, which is located within the western portion of the Abitibi, is responsible for 37% of the total gold and 21% of the total base metal production of the Abitibi greenstone belt (e.g., Franklin and Thorpe, 1982; Spooner and Barrie, 1993). Volcanogenic massive sulfide deposits in the Abitibi formed between ca. 2750 and 2695 Ma (Ayer et al., 2002; Thurston et al., 2008; McNicoll et al., 2014; Ross et al., 2014), and correspond to seven geochronologically defined episodes of volcanism (Fyon et al., 1991; Hannington et al., 1999a; Thurston et al., 2008).

3. Geological setting of the Kidd Creek deposit

The Kidd-Munro assemblage (2720–2710 Ma) is a 200 km long, east-west trending belt of mafic, ultramafic and felsic metavolcanic rocks that extends for at least 100 km from Timmins, Ontario eastward into the province of Quebec (Jackson and Fyon, 1991; Berger et al., 2011). It consists of basaltic komatiites, pyroxenites, Fe- and Mg-rich tholeiites, high alumina basalts, numerous high-level mafic-ultramafic intrusive complexes, peridotitic komatiites, and minor high silica rhyolite and interflow sediments (Jackson and Fyon, 1991). The felsic volcanic rocks of the Kidd-Munro assemblage have been dated at ca. 2719 to 2710 Ma (Nunes and Pyke, 1980, 1981; Corfu et al., 1989; Barrie and Davis, 1990; Jackson and Fyon, 1991; Corfu, 1993; Bleeker and Parrish, 1996; Ayer et al., 2002, 2005; Berger et al., 2007; Bleeker and van Breeman, 2011) and the maximum age of the rhyolite units at Kidd Creek is 2716.5 ± 1.0 Ma (Bleeker and van Breeman, 2011). This indicates that the rhyolites at Kidd Creek are time correlative with bimodal mafic-ultramafic and felsic suites to the east and north suggesting that the tectonic and magmatic events responsible for local rhyolitic volcanism within the predominantly mafic-ultramafic volcanic environment occurred at approximately the same time on a regional scale.

The Kidd-Munro strata are subvertical and occupy large east-trending folds (Ludden et al., 1986; Barrie and Davis, 1990; Bleeker et al., 1999; Dinel et al., 2008). Immediately south of the Kidd-Munro assemblage is the Porcupine Group (ca. 2699 Ma), an east-trending belt of turbidic greywackes (Bleeker and Parrish, 1996; Bleeker et al., 1999) that unconformably overlie the Kidd-Munro assemblage. In the Kidd Creek mine area, the contact between the Kidd-Munro assemblage and the Porcupine Group is steep, faulted and interpreted to represent a faulted and folded unconformity (Bleeker, 1995; Bleeker and Parrish, 1996). The Kidd-Munro assemblage is bound to the north by ca. 2725 Ma volcanic rocks of the Deloro assemblage (Mortensen, 1993; Ayer et al., 2002). To the west, the Kamiskotia volcanic complex of the Tisdale assemblage has a poorly defined contact with the Kidd-Munro assemblage (Bleeker, 1999). Immediately north of Timmins, the Kidd-Munro assemblage comprises the Kidd Volcanic Complex (Bleeker and Parrish, 1996).

The Kidd Volcanic Complex covers several hundred square kilometers, extending for 10 to 20 km east and west of the mine. It is comprised of a strongly bimodal suite of komatiitic flows and high silica rhyolite, overlain by tholeiitic basalt (Bleeker, 1999). Sedimentary rocks form only a small portion of the Kidd Volcanic Complex and are represented by thin, interflow graphitic argillites, siltstones and felsic tuff units (Bleeker, 1999). The Kidd Volcanic Complex differs from the rest of the Kidd-Munro assemblage in that it contains a greater proportion of rhyolitic volcanic rocks (10–20%) and lacks rocks of intermediate (55–70 wt% SiO_2) composition (Bleeker, 1999). The depositional environment for the Kidd Volcanic Complex has been interpreted as subaqueous based on pillowed mafic flows, and argillaceous sediment (Bleeker, 1999). Comba et al. (1986), however, described Strombolian-type basaltic tephra deposits, which they interpreted to indicate that part of the Kidd Volcanic Complex may have formed in a subaerial or shallow subaqueous environment. Based on these observations Bleeker (1999) interpreted the paleovolcanic environment of the Kidd Volcanic Complex to be a complex mixture of deep-water, shallower water and possibly emergent volcanic environments.

Rocks of the Kidd Volcanic Complex and the Porcupine Group define an S-asymmetric, north-trending regional fold that has refolded the southern limb of a preexisting, upright syncline, thereby changing the east trend of the Kidd-Munro assemblage (Bleeker, 1999). The Kidd Creek deposit sits on the limb of a north-trending parasitic structure on the regional fold (Fig. 2; Bleeker, 1999). To the north and west of the mine are two large structural basins, the Kidd 66 and Kidd West respectively, that are a result of a large-scale fold interference pattern created by east-trending F_0 synclines and steeply northeast-plunging F_1

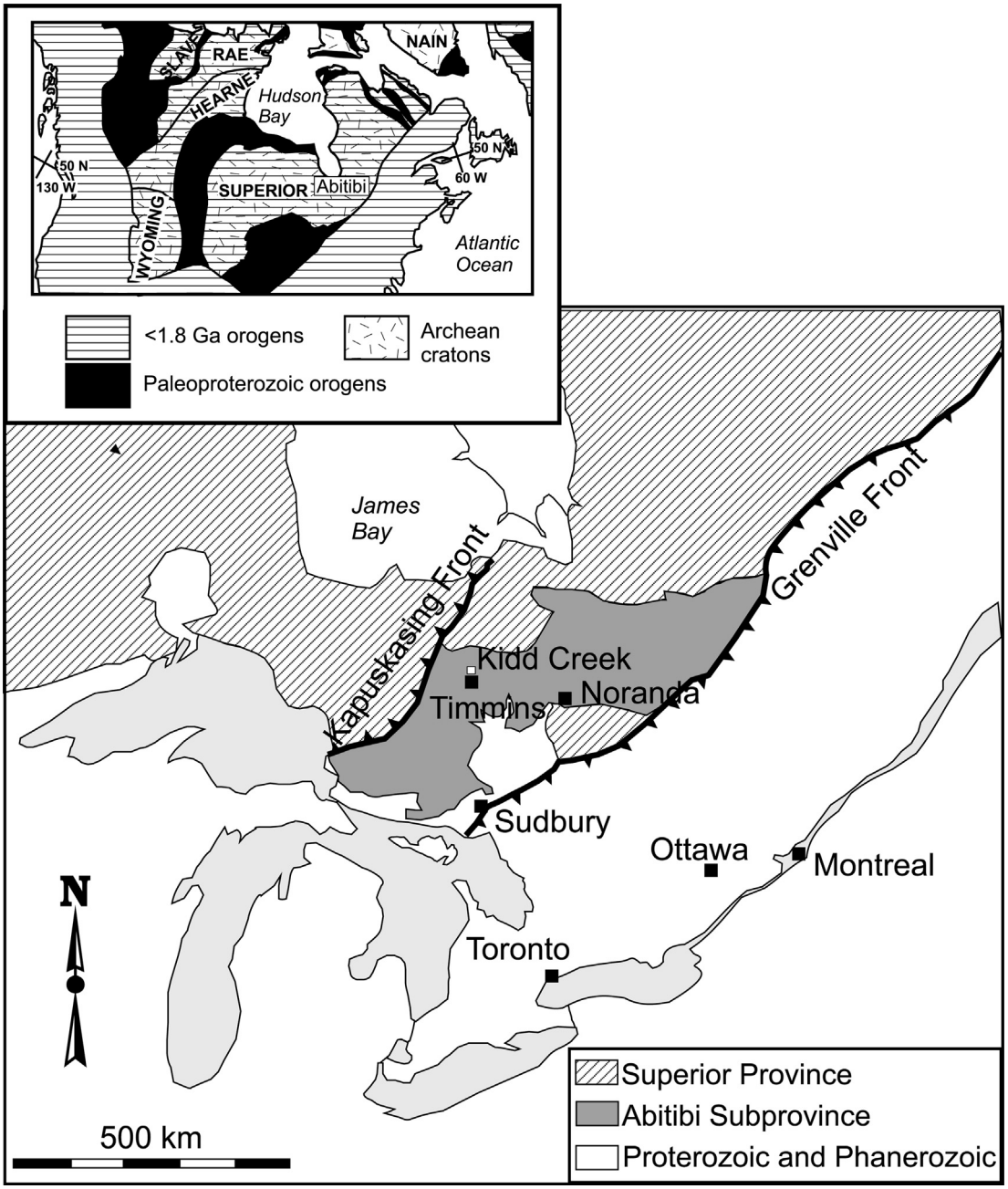

Fig. 1. General geology map showing the Abitibi greenstone belt and the location of the Kidd Creek mine approximately 24 km north of Timmins (modified from Bleeker and Hester, 1999). The inset map shows the location of the Abitibi Subprovince within the Superior province.

fold axes (Bleeker, 1999; Hannington et al., 1999a). The basins are large synforms comprised of basaltic pillow lavas, mafic breccias, and minor interflow sediments and felsic volcaniclastic rocks. The mafic volcanic rocks of the Kidd 66 basin occur in the stratigraphic hanging-wall of the Kidd Creek deposit and are broadly correlative across the Kidd West and Kidd 66 basins. Mafic volcanic rocks of the Kidd 66 basin conformably overlie the NR (Hannington et al., 1999a).

In the Kidd 66 and Kidd West basins there are several time-equivalent rhyolitic volcanic and interflow volcanic-sedimentary rocks including the Chance and Fly Creek rhyolitic units (Fig. 2). Rhyolitic units on the north side of the Kidd 66 basin face south, and near the mine they face north and west. This suggests that the rhyolitic units are related by folding and that the Chance rhyolite and the NR are time-stratigraphic equivalents of the Kidd Creek mine rhyolite and therefore may be an extension of the Kidd Creek mine stratigraphy (Bleeker et al., 1999).

4. Geology of the Kidd Creek mine area

In the Kidd Creek mine area, D_1 is the dominant deformation, and manifests as large-scale F_1 folds, such as the isoclinal and overturned Kidd Creek mine fold that plunges 70° towards 020° (Fig. 2). The predominant S_1 cleavage is northwest trending, dips steeply to the northeast (60–80°), and locally may show a change in trend of up to 90°, which is attributed to a later re-folding (F_2) of an originally axial planar S_1 cleavage (Bleeker, 1999). Stratigraphy at the Kidd Creek mine, which is located on the south limb of the F_1 fold, is overturned and youngs to the west. The Kidd Creek orebodies are elongate parallel to the F_1 hinge that also coincides with a primary volcanic rhyolite ridge that underlies the orebodies (Prior, 1996; Prior et al., 1999a; Bleeker, 1999). The F_2

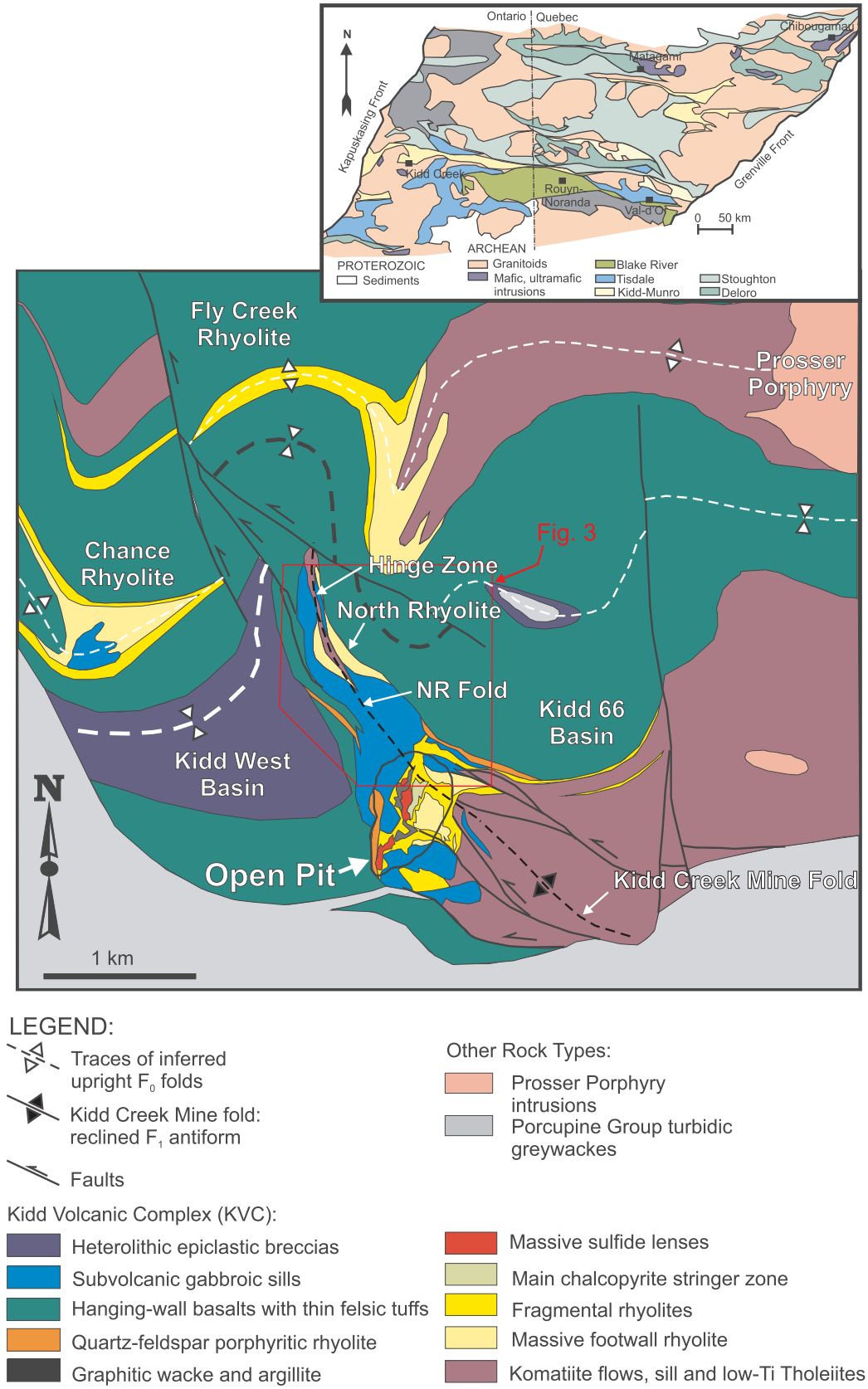

Fig. 2. Geological map of the Kidd Creek area showing the NR in relation to the Kidd mine (after Bleeker, 1999). The NR fold represents the continuation of the Kidd Creek mine fold anticlinal axis as defined during this study through drill hole data and projected to surface from 3200 foot level. The inset map shows the location of the Kidd Creek deposit within the Abitibi Subprovince. The red outline marks the location of the map in Fig. 3. (For interpretation of the references to colour in this figure legend, the reader is referred to the web version of this article.)

fold axes are subparallel to F_1 fold axes, which result in a coaxial fold interference pattern that has further enhanced the cylindrical nature of the orebodies (Bleeker, 1999).

Volcanic stratigraphy in the Kidd Creek mine area has an approximate thickness of 2.6 km, including 1 km of footwall ultramafic flows, < 200 m of rhyolitic rocks, and ≥1.5 km of basaltic hanging-wall rocks (Bleeker, 1999). Before tectonic deformation, the footwall komatiitic flows presumably formed a relatively flat lava plain on which rhyolitic flows and volcaniclastic rocks were extruded and deposited.

Barrie (1999) interpreted the Kidd Creek komatiites to represent a vent proximal environment because of their similarity to the channelized flow facies at Kambalda. He cited the occurrence of: (1) ultramafic dykes and dykelets; (2) a chaotic footwall stratigraphic succession; (3) the spatial coincidence of proximal rhyolite flows; (4) hanging-wall basalt feeder dykes; (5) a long-lived graben-like depression; and (6) a giant hydrothermal system vent area, as evidence to support the interpretation that the Kidd Creek komatiites were erupted from a proximal fissure or vent. Barrie (1999) suggested that the komatiites were extruded into a "graben-like depression" that was later covered by the mine rhyolites. The ultramafic flows are locally intercalated with older rhyolites indicating that ultramafic volcanism was still active when the first high-silica rhyolites were extruded (Bleeker, 1999). Overlying the ultramafic flows are massive, weakly quartz to feldspar phyric (1–3%) high-silica rhyolites that, in turn, are overlain by a succession of autoclastic rhyolite breccias, lapillistones and lapilli tuffs (Prior et al., 1999a). These strongly silicified, in situ rhyolite breccias and rhyolite volcaniclastic rocks host the main copper stringer zone and the massive sulfide orebodies.

Conformably overlying the bedded rhyolite volcaniclastic units is a massive quartz porphyritic (QP) rhyolite. The QP rhyolite and its associated in situ breccia and volcaniclastic rocks commonly contain 5 to 20%, 1–5 mm, euhedral quartz crystals, but may contain up to 35% quartz crystals (Prior et al., 1999a). The QP rhyolite is interpreted to mark the beginning of hanging-wall volcanism to the Kidd Creek massive sulfide deposit (Prior et al., 1999a). At the Kidd Creek mine the QP rhyolite is locally sericite altered and mineralized (pyrite-sphalerite) and its age of 2716.3 ± 1.0 Ma completely overlaps with that of the footwall rhyolite (Bleeker and van Breeman, 2011). Interflow felsic tuffs from the youngest basalt flows of the hanging-wall have an age of 2714.8 ± 0.7 Ma, meaning that rhyolitic volcanism at Kidd Creek lasted ~2 million years at most and possible much less when considering the full error envelope on the U-Pb zircon ages. Basaltic flows directly above the QP rhyolite show only weak hydrothermal alteration and are not mineralized, consistent with their emplacement during the waning stages of hydrothermal activity (Huston et al., 1995; Bleeker and Parrish, 1996; Bleeker et al., 1999; Prior et al., 1999a).

The entire mine sequence is intruded by irregular synvolcanic gabbroic sills. Peperite developed along the sill margins indicate that the subhorizontal gabbroic sills are comagmatic with the compositionally identical overlying basalts and separate the massive and volcaniclastic aphyric rhyolite from the QP rhyolite (Prior et al., 1999a). The abundance of these sills in the Kidd Creek mine area, on the southern limb of the Kidd Creek mine F_1 fold, supports the interpretation that it is a proximal volcanic environment for hanging-wall basalt volcanism.

The Kidd Creek orebodies are interpreted to have formed in a linear graben or half-graben as a series of stacked lenses and are accompanied by a rapid lateral change in thickness and facies of the footwall and hanging-wall rhyolites (Bleeker, 1999). The size and morphology of this depression is unknown; however, Bleeker (1999) proposed that one structural margin of the inferred graben, or half-graben, may lie within the F_1 fold axis of the NR.

5. Methodology

Poor surface exposure in Kidd township required that the NR study be based on a combination of drill core logging and underground mapping coupled with systematic sampling of all lithofacies within the NR and followed by detailed petrographic and high precision lithogeochemical analyses.

In the lithofacies descriptions and discussions that follow, the term volcaniclastic refers to *"all clastic volcanic materials formed by any process of fragmentation, dispersed by any kind of transporting agent, deposited in any environment or mixed in any significant portion with nonvolcanic fragments"* (Fisher, 1961). The terms tuff, lapilli-tuff, lapillistone, and tuff-breccia are non-genetic, granulometric classifications related to the %age and size of the components, and do not imply a pyroclastic origin (Fisher, 1961; Schmid, 1981; White and Houghton, 2006).

5.1. Core logging and underground mapping

Thirty drill holes, totaling ~30 km, were selected for this study such that they covered the entire NR with a minimum x and y spacing of 400 m. Detailed (1:500) logging of the lithofacies present in the core was done and graphically portrayed to better understand the stratigraphy and volcanology of the NR. An additional 20 drill holes, logged by mine geologists, were selected to insure complete coverage of the NR and this data was used in the volcanic reconstruction of the NR.

The ~650 m long 2800 Level exploration drive at Kidd Creek intersected (it is no longer accessible) the NR stratigraphy and was also mapped in detail (1:500) to help understand of the stratigraphy and structure of the NR. Each lithological unit was described in terms of primary textures, mineralogy and alteration. Alteration, foliation, and faults were documented and measured in order to understand the deformational history of the NR. A map of the upper surface of the drift (the "back") that displayed the best cross-sections perpendicular to the stretching lineation (Appendix A, Fig. A.1) Six detailed wall maps (1:100) were drawn to document important contacts, structures and textures. Two will be referenced in the text below and four can be found in Appendix A (Figs. A.2–A.5). Underground mapping and detailed core logging data were used in the volcanic reconstruction.

5.2. Petrology

Detailed petrography was completed on 51 drill core samples representing all major lithofacies in the NR stratigraphy. General textures and mineralogy are contained in the lithofacies descriptions below, and detailed petrographic descriptions are included in Appendix B.

5.3. Geochemical analyses

A whole rock geochemical database of samples systematically collected from drill core was provided by the Kidd Creek Division of Falconbridge Limited (now Glencore Ltd.) and is contained in Appendix C (Table C.1). All whole rock data are given as raw data in the supplemental datasets (above and below), but the data were recalculated volatile free to 100% for the comparisons and diagrams using whole rock geochemistry herein. Samples from the Falconbridge Ltd. database were gathered from 1970 to 2001. All samples analyzed prior to 1992 (diamond drill holes with numbers lower than 5000) were done by X-Ray Assay Laboratories (XRAL, Don Mills, ON) and from 1993 onwards the whole rock analyses were done by TSL/Assayers Laboratories (Missasauga, ON). Major oxide analyses were done by X-ray florescence spectroscopy with a fused disc prepared from a 2 g sample. XRAL and TSL detection limits are 0.01 wt% for majors. The detection limit at TSL for trace elements is 10 ppm and at XRAL the detection limit for Ba, Nb, Rb, Sr, Y, and Zr is 2 ppm and Ba is 20 ppm. The Falconbridge database was used for alteration and mineralization studies only.

To augment the data set provided by Falconbridge Ltd. and allow

comparison with high quality published data, 46 samples collected from drill core during this study were analyzed for major and trace geochemistry and are included in Appendix C (Table C.2). Sample preparation and analysis were completed by the Ontario Geoscience Laboratories, Sudbury, Ontario. Samples were pulverized in a steel jaw crusher and subsequently powdered in an agate mill. Total abundances of major oxides were analyzed by XRF. The calcined samples were fused with a borate flux to produce a glass bead for analysis. Replicate analyses of samples and standards reveal relative standard deviations (% RSD) of < 18% for XRF determinations. Samples analyzed for trace elements underwent a closed beaker digest using four acids (hydrofluoric, hydrochloric, perchloric, and nitric acids) to ensure total dissolution of all solids. The samples were then analyzed for trace elements using inductively coupled plasma-mass spectrometry (ICP-MS). Replicate analyses of samples and standards reveal relative standard deviations (%RSD) of < 10% for ICP-MS determinations.

6. Geology of the North Rhyolite

The aphyric rhyolite of the NR has similar U-Pb zircon age (2716.0 ± 0.5 Ma) to that of the aphyric rhyolite (2716.5 ± 0.7 Ma) of the Kidd Creek mine stratigraphy and has therefore been interpreted to represent a lateral extension of the Kidd Creek mine stratigraphy (Bleeker et al, 1999; Bleeker and van Breeman, 2011). Bleeker (1999) also proposed that faults that slice through the Kidd Creek mine fold have displaced the northern limb of the Kidd Creek mine fold up to 2 km to the northwest. This implies that the NR is the continuation of the Kidd Creek mine stratigraphy but has been displaced through faulting.

Detailed underground mapping and drill core logging indicate that the stratigraphy of the NR is identical to that of the Kidd Creek mine stratigraphy. From oldest to youngest, the stratigraphy of the NR and Kidd Creek mine area includes: komatiitic flows with interflow rhyolites, massive aphyric rhyolite, brecciated aphyric rhyolite, aphyric rhyolitic volcaniclastic rocks, massive QP rhyolite, QP rhyolite volcaniclastic rocks, and low and high TiO_2 basalt flows (Fig. 3). Facing reversals within the komatiitic flows over a distance of approximately 10 m have been used to define the hinge of a major anticline within the NR (Fig. 4). Ranges in whole rock major and trace element chemistry for the dominant rock types in the NR are given in Table 1.

6.1. Ultramafic lithofacies

The ultramafic rocks are up to 150 m-thick in the NR (Fig. 3). They are divisible into two units based on grain size and texture. The first is a coarse-grained ultramafic unit that has a maximum thickness of 80 m. The second is a fine-grained ultramafic unit (≤100 m thick) comprised of komatiitic flows with distinct flow top breccias. Both the coarse-grained and fine-grained ultramafic rocks of the NR are strongly talc and carbonate altered, generally comprised of talc, calcite, quartz and seldom serpentine (no primary mineralogy remains).

6.1.1. Coarse grained ultramafic lithofacies

The coarse-grained ultramafic unit has a gradational upper contact (over ~1 m) with the komatiitic flows, but locally a faulted upper contact with massive aphyric rhyolite. The coarse-grained ultramafic lithofacies is light grey to beige, and dominated by 5–7 mm, pale grey to brown serpentine after olivine crystals in a very fine grained matrix of talc, calcite, quartz and fucsite; Fig. 5a, b).

6.1.2. Komatiite lithofacies

The komatiite occurs stratigraphically below the massive aphyric rhyolite, and is laterally discontinuous, forming elongate, sheared lozenges of fine-grained ultramafic rock in the core of the NR anticline. The contact with overlying rhyolite is sharp, strongly sheared and locally intercalated with massive rhyolite where contacts are sharp and irregular, or brecciated. The komatiite lithofacies is fine-grained, black, and contains polygonal flow top breccias. Fragments within the breccia are ~10 cm in size, but decrease in size toward the flow top, which is marked by hyaloclastite (Fig. 5c, d).

6.2. Aphyric rhyolite lithofacies

The aphyric rhyolite unit is up to 100 m thick in the NR (Fig. 3). It is underlain by ultramafic flows and is typically intruded by synvolcanic gabbroic sills and dykes. The aphyric rhyolite is stratigraphically below the QP rhyolite and where the QP rhyolite is absent the aphyric rhyolite is conformably overlain by basaltic flows or mafic volcaniclastic rocks. The lower 10 m of the basal basalt flow seldom contains blocks of aphyric rhyolite. The aphyric rhyolite is subdivided into three lithofacies: massive (commonly flow banded), in situ breccia, and breccia.

6.2.1. Massive aphyric rhyolite lithofacies

This lithofacies is homogeneous, medium grey in colour, and generally aphyric with only minor quartz (5% round to angular, 1 mm, grey) and feldspar (1%, euhedral to anhedral, 1 mm, white) phenocrysts. The aphyric groundmass is a mix of very fine grained quartz and feldspar variable replaced by sericite (Fig. 6a). The lithofacies is locally flow banded (mm to cm wide, orange and grey bands) and seldom spherulitic. Occurrences of this lithofacies range from 5 to 80 m in thickness.

6.2.2. In situ brecciated aphyric rhyolite lithofacies

This lithofacies contains white to grey, angular and round, aphyric, seldom weakly quartz and feldspar phyric rhyolite fragments in a dark grey to pale yellow matrix. Fragments range in size from 40 cm to < 1 cm, may be flow banded, and are tightly packed, have a jig-saw puzzle fit, and are separated by only a 1–3 mm, commonly dark green and, less commonly yellow, matrix of very fine-grained chlorite and sericite respectively (Fig. 6b). Overall this lithofacies is mottled in appearance due to overprinting of patchy silicification. Occurrences of this lithofacies range from < 5 to 80 m in thickness.

6.2.3. Brecciated aphyric rhyolite lithofacies

This lithofacies is characterized by white to pale grey to pale yellow, round to angular, rotated, aphyric rhyolite fragments that are generally < 40 cm, but can be up to 5 m across (Fig. 6, d). The rhyolite fragments are composed of very fine grained quartz, and feldspar variably replaced by sericite. The matrix is also composed of very fine grained quartz and feldspar, but is commonly replaced by very fine grained chlorite or sericite. Locally this lithofacies contains ≤5% disseminated to stringer-style pyrrhotite and pyrite (Fig. 7). Very rarely the lithofacies contains basalt clasts. Occurrences of this lithofacies range from 1 to 30 m in thickness.

6.3. Felsic volcaniclastic lithofacies

The felsic volcaniclastic unit is up to 62 m-thick in the NR (Fig. 3) and can be subdivided into three lithofacies dominated by aphyric rhyolite clasts: rhyolite tuff breccia, rhyolite lapilli tuff and rhyolite tuff. The lithofacies commonly contain < 5% disseminated pyrite and pyrrhotite (< 5 mm) and is locally mineralized, containing ≤5% disseminated pyrite and pyrrhotite, and ≤ 5% chalcopyrite as stringers (cm-scale). The felsic volcaniclastic lithofacies is overlain by massive QP rhyolite, mafic volcaniclastic, or basalt depending on location. It is underlain by an in situ aphyric rhyolite breccia.

6.3.1. Rhyolite tuff breccia lithofacies

This lithofacies is grey to pale grey, containing approximately 30% round, flow banded, blocks (> 64 mm) and 50–65% round, lapilli of white, massive, aphyric rhyolite in a dark green to yellow very fine grained matrix of quartz, sericite and chlorite. Occurrences of this

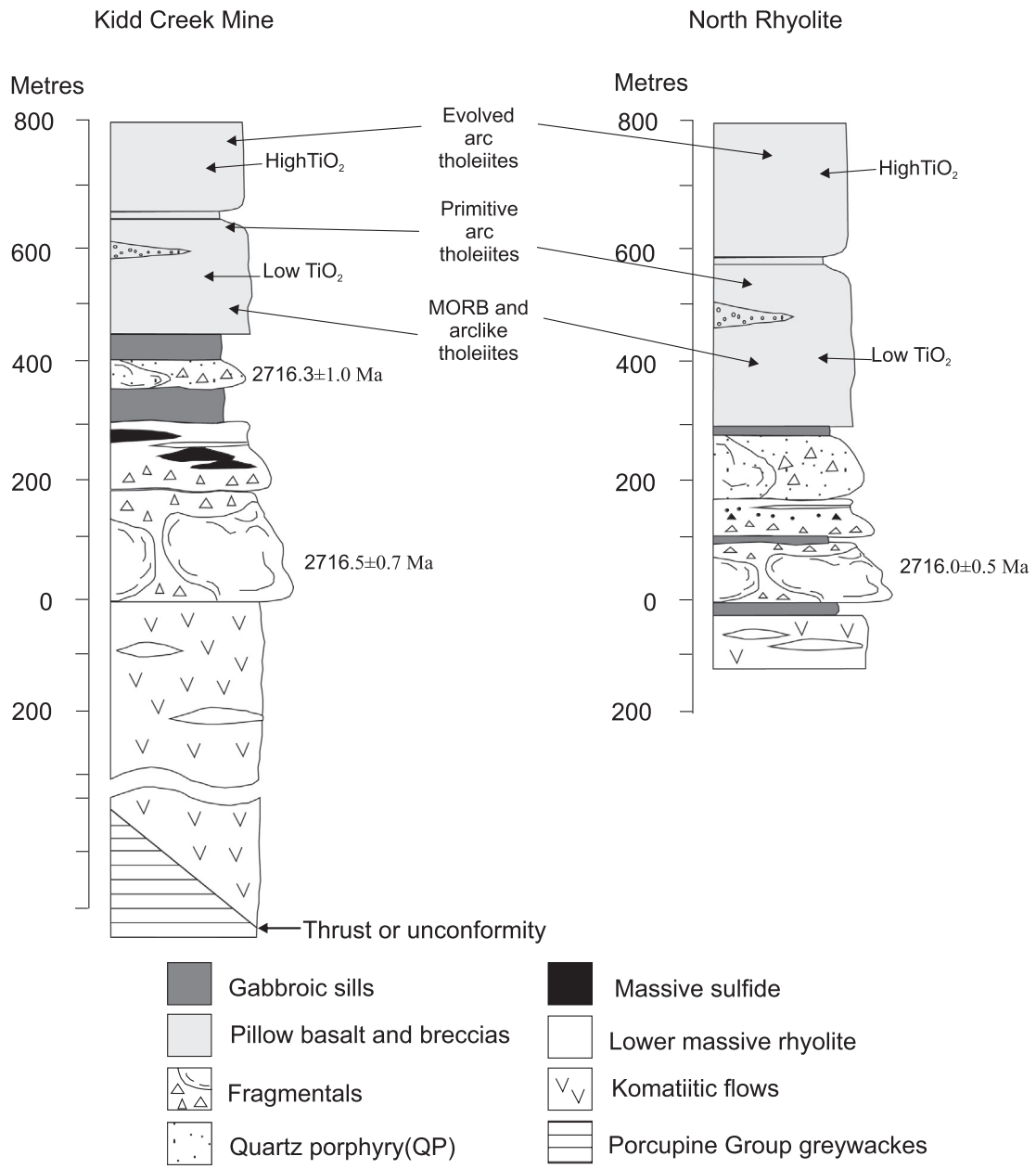

Fig. 3. Generalized stratigraphy of the Kidd Creek mine (Prior et al., 1999) and the North Rhyolite (this study) showing the U-Pb zircon ages of different units with the mine stratigraphy (Bleeker et al, 1999, and Bleeker and van Breeman, 2011). Note: basalt flows of the NR continue for another ~800 m above the stratigraphy shown in this section.

lithofacies range from < 5 m to 30 m thick and individual beds are < 1–5 m thick and massive.

6.3.2. Rhyolite laplli-tuff lithofacies

This lithofacies comprises white and grey, round to subround, aphyric rhyolite lapilli (2–64 mm, average < 2 cm) in a dark green to yellow matrix made of fine-grained quartz, sericite and chlorite (Fig. 6e, f). Occurrences of this lithofacies range from < 1 to 62 m thick with individual beds ranging from 1 to 20 cm in thickness. These are commonly massive or normally graded with reverse grading rare.

6.3.3. Rhyolite tuff lithofacies

This lithofacies commonly contains < 10%, pale grey to yellow, round, rhyolite lapilli (< 4 cm) and ≤5% quartz crystals (subround, < 5 mm) in very fine grained quartz and sericite. Locally quartz crystal-rich beds containing 10–20%, 1 to 2 mm angular to rounded quartz crystals are present. Overall the lithofacies is finely laminated (mm-scale) with occurrences ranging from < 1 to 10 m thick.

6.4. Heterolithic volcaniclastic lithofacies

Heterolithic volcaniclastic rocks are not common and range from < 1 m to 10 m thick in the NR. They comprise two lithofacies: heterolithic lapillistone and a rhyolitic tuff breccia containing mafic blocks. The lithofacies occur stratigraphically below the massive QP rhyolite, mafic volcaniclastic, or basalt lithofacies where the QP rhyolite is absent. A gabbro sill typically occurs at the upper contact between the heterolithic volcaniclastic unit and the QP rhyolite. The lower contact with the underlying felsic volcaniclastic rocks or brecciated aphyric rhyolite is sharp and conformable. Beds of heterolithic volcaniclastic lithofacies seldom occur within felsic volcaniclastic rocks.

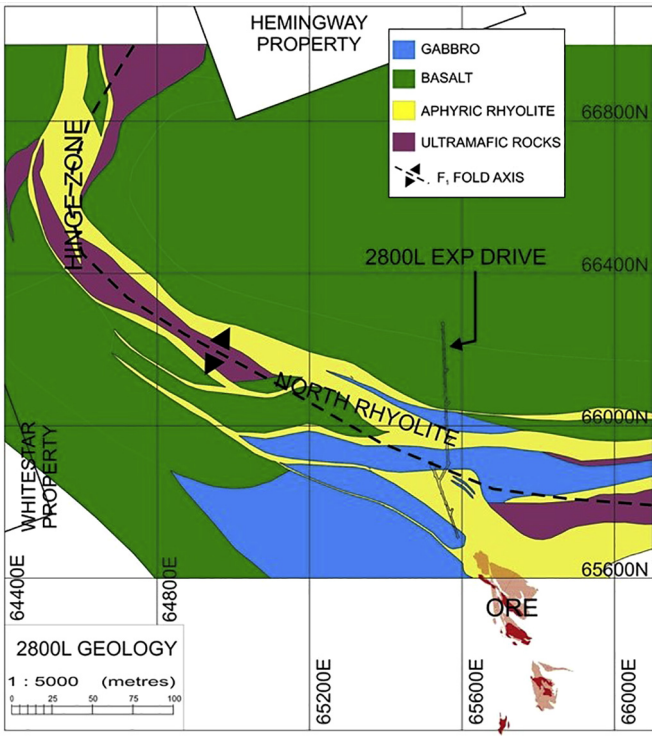

Fig. 4. Geology of the 2800 Level, showing the NR including location of the 2800 Level exploration drift, and the Kidd Creek orebodies. The dashed line represents the NR anticlinal axis projected from 3200 Level and further defined through drill hole data.

6.4.1. Heterolithic lapillistone lithofacies

The lapillistone beds are less than 20 cm thick and are dominated (60–85%) by grey, round to angular, aphyric rhyolite lapilli, ≤10% round, pale grey-brown, lapilli- to block-sized basalt clasts, < 1% round, < 3 mm, quartz crystal clasts and < 1% angular, lapilli-sized mudstone clasts (Fig. 8a). No primary mineralogy remains in the basalt clasts, it is replaced by calcite and quartz. The rhyolite clasts are very fined grained quartz and sercicite. The matrix is very fine grained sericite, calcite and quartz. Individual beds within this lithofacies are normally graded or massive and 1–20 cm thick.

6.4.2. Heterolithic tuff breccia lithofacies

The heterolithic tuff breccia lithofacies is characterised by ≤25%, pale grey-brown, round basalt and ~10% pale grey to white, strongly silicified, round, rhyolite lapilli and blocks in a matrix of very fine grained quartz, sericite and calcite. Individual beds within this lithofacies are massive and 1–20 cm thick.

6.5. Quartz porphyritic (QP) rhyolite lithofacies

The QP rhyolite is up to 113 m-thick in the NR (Fig. 3). A large synvolcanic gabbroic sill commonly marks the contact between QP rhyolite and the underlying aphyric rhyolite. The upper contact of the QP rhyolite is conformable with a mafic volcaniclastic unit displaying a mix of QP rhyolite and basalt clasts. Where the mafic volcaniclastic unit is absent, the QP rhyolite is in conformable contact with pillow basalt that contains blocks of QP rhyolite in its basal 10 m. The QP rhyolite comprises three distinct facies: massive rhyolite, in situ rhyolite breccia, and rhyolite breccia, which have gradational contacts over 1–5 m.

6.5.1. Massive QP rhyolite lithofacies

This lithofacies is dark grey to pale yellow and is characterized by 10–25% euhedral to subhedral, grey, 1–4 mm, quartz phenocrysts (Fig. 8b). Locally the lithofacies contains ≤5% euhedral, white, 1–4 mm, feldspar phenocrysts (Fig. 8c). The groundmass of very fine grained quartz and feldspar is variably replaced by sericite and calcite. Despite the alteration, spherultites are regularly preserved in this lithofacies. Locally it is flow banded with mm- to cm-wide, orange and grey bands comprised of very fine grained quartz, feldspar and sericite. Occurrences of the massive lithofacies range from 5 to 113 m.

6.5.2. In situ QP rhyolite breccia lithofacies

This lithofacies is characterized by white to grey to pale yellow, angular to round QP (5–20% euhedral to subhedral, ≤3 mm quartz phenocrysts) rhyolite fragments that are tightly packed with a “jig-saw puzzle fit” and are separated by 1–3 mm of pale yellow to dark green matrix of very fine grained quartz, feldspar and sericite or chlorite. Fragments range in size from < 1–0 cm, are composed of very fine grained quartz and sericite, and are seldom flow banded. Strong to moderate silica alteration commonly gives the rock a mottled texture or appearance. Occurrences of the in situ QP rhyolite breccia lithofacies range from 1 to 60 m.

6.5.3. QP rhyolite breccia lithofacies

This lithofacies is characterized by grey to pale yellow QP (5–10%, euhedral to subhedral, 1–3 mm quartz phenocrysts) rhyolite clasts (60–75%, 1–25 cm, very fine grained quartz and feldspar) in a very fine grained matrix of sericite, quartz and minor feldspar. Occurrences of the in situ QP rhyolite breccia lithofacies range from < 1–50 m.

6.6. Argillite lithofacies

Argillaceous rocks generally occur as < 1 m thick, graphitic interbeds within rhyolite volcaniclastic lithofacies near or at the top of the aphyric rhyolite, or as interflow sediments within the hanging-wall basalt. They are black to dark grey, very fine-grained, and massive to finely laminated and seldom contain dark grey, round rhyolite (< 5%, ≤2 cm), pyrite (< 2%, ≤2 cm), and pyrrhotite (< 2%, ≤2 cm) clasts.

6.7. Peperite lithofacies

The peperite lithofacies ranges in thickness from 1 to 60 m and comprises a complex mix of mafic clasts in an aphyric rhyolite breccia matrix (Fig. 8d). Mafic clasts range in size from 2 mm to several meters, have fluidal shapes and chilled margins (1–3 mm) commonly with hyaloclastite concentrated along their margins. The lithofacies also contains dykes and dyklets (≤2 m) of very fine grained, pale green mafic rocks that often have chilled fluidal margins that contain hyaloclastite. In the 2800 Level exploration drift this lithofacies contained 1–4 cm wide stingers of pyrite and pyrrhotite (Fig. 9). This lithofacies commonly occurs where the felsic volcaniclastic lithofacies is in direct contact with the overlying basalt (i.e. where the QP rhyolite does not occur).

6.8. Mafic volcaniclastic lithofacies

The mafic volcaniclastic unit (Fig. 6e) is < 15 m thick, laterally discontinuous, and occurs between the QP or aphyric rhyolite, and the overlying basaltic flows, or between basalt flows. The unit is crudely bedded (1–2 m) with both matrix-supported and clast-supported beds. It contains ~60% round, 1–10 cm, pale green to grey, fine grained mafic fragments, ~15% round, rhyolite lapilli, and ~5% round, < 1–2 cm clasts of very fine grained pyrite and pyrrhotite in a very fine grained, dark green matrix of chlorite, calcite and quartz.

6.9. Basalt lithofacies

A voluminous basaltic sequence (> 1 km thick, Fig. 3) occurs at the top of the NR stratigraphy. It occurs on both limbs of the NR anticline. The basalt is generally pillowed (Fig. 8f), with lesser amounts of

Table 1
Ranges in composition for units of the North Rhyolite.

	Coarse Grained Ultramafic	Komatiite	Aphyric Rhyolite	QP Rhyolite	Basalt
SiO_2 (wt%)	26–34	21–35	72–87	70–85	43–46
TiO_2	0.15–0.18	0.09–0.18	0.60–0.21	0.10–0.17	0.03–2.7
Al_2O_3	2.9–16.7	2.0–3.3	7.2–13.2	8.3–14.6	17.2–19.8
Fe_2O_3	6.9–8.7	5.7–8.2	0.2–4.8	0.7–3.3	8.7–11.6
MnO	0.08–0.17	0.08–0.20	0.01–0.05	0.02–0.14	0.25–0.32
MgO	23.5–33.7	23.8–33.5	0.2–5.6	0.1–3.2	2.6–4.3
CaO	0.1–2.1	0.4–11.5	0.2–2.1	0.3–2.9	11.5–12.8
Na_2O	0.02–0.18	0.02–0.04	0.1–7.6	0.1–7.0	2.1–2.6
K_2O	0.22–3.03	–	0.14–4.15	0.29–5.04	0.01–1.18
P_2O_5	0.02	0.03	0.01–0.2	0.01–0.2	0.01–0.52
LOI	22.4–28.8	20.0–31.7	0.7–3.9	0.9–4.8	5.0–7.4
ppm					
Ni	95–1704	1166–2002	< 4–116	< 4–147	191–211
Sc	8.5–35.5	5.7–11.0	0.7–7.2	1.1–4.1	28.3–31.1
V	27.4–144.0	29.0–53.8	< 0.6–52.3	< 0.6–22.0	214.0–240.6
Rb	0.5–7.1	0.3	5.1–150.0	7.9–141.7	0.1–48.5
Cs	0.19–0.38	0.21–0.35	0.40–3.03	0.25–2.86	0.15–1.52
Sr	8.1–53.5	2.7–115.6	9.3–64.4	13.9–78.6	82.3–129.5
Nb	0.2–0.9	≤0.3	4.9–24.2	10.4–21.4	1.5–1.7
Hf	0.2–0.5	0.1–0.4	2.1–10.3	5.2–9.8	1.1–1.2
Zr	7–13	5–12	62–274	156–281	34–42
Y	2.7–7.7	1.9–4.5	27.0–120.0	30.5–84.4	16.2–18.7
Th	< 0.06–0.11	≤0.6	2.06–8.66	4.91–8.85	0.12–0.14
U	0.01–0.03	0.01–0.02	0.50–2.25	0.92–2.01	0.03–0.04
La	0.50–0.86	0.38–0.59	12.93–58.33	20.45–54.66	1.73–2.31
Ce	1.14–2.22	0.79–1.49	30.07–126.15	33.54–115.2	5.27–5.72
Pr	0.17–0.35	0.12–0.23	3.59–17.41	3.52–15.14	0.88–0.91
Nd	0.93–1.86	0.60–1.10	13.17–73.04	12.84–59.38	4.64–4.99
Sm	0.33–0.65	0.18–0.43	2.90–17.84	2.56–13.34	1.65–1.80
Eu	0.09–0.24	0.07–0.25	0.45–2.63	0.81–2.15	0.63–0.75
Gd	0.44–1.10	0.30–0.59	3.16–19.43	2.91–12.32	2.30–2.57
Tb	0.09–0.20	0.06–0.12	0.53–3.38	0.49–2.08	0.41–0.47
Dy	0.45–1.32	0.34–0.78	3.62–20.00	3.70–13.32	2.87–3.06
Ho	0.11–0.31	0.10–0.17	0.90–4.65	0.93–3.08	0.62–0.72
Er	0.39–0.92	0.28–0.49	2.70–13.93	3.09–9.38	1.82–2.10
Tm	0.06–0.14	0.04–0.08	0.42–2.13	0.53–1.51	0.26–0.34
Yb	0.31–0.86	0.29–0.43	2.67–12.58	3.35–9.63	1.71–2.18
Lu	0.06–0.13	0.04–0.07	0.40–2.06	0.49–1.35	0.27–0.34

Note: LOI, loss on ignition.

massive flows (locally *in-situ* brecciated), pale to dark green, aphyric and locally plagioclase phyric (< 5%, ≤1 mm). Both pillow and massive lithofaceis are moderately to strongly chloritized and carbonitized with near complete replacement of the quartz, feldspar, and pyroxene by chlorite and calcite. The pillowed lithofacies contains 1–20%, 1 mm, chlorite filled amygdules that increase in abundance towards pillow margins. Pillow selvages are 1–5 cm wide, often contain hyaloclastite and consist of very fine grained chlorite and calcite.

7. North Rhyolite versus Kidd Creek volcanic environments

The following is a discussion of the petrogenesis and mechanisms of emplacement of the main lithofacies of the NR, with some comparisons to the correlative units within the Kidd Creek mine stratigraphy.

7.1. Ultramafic lithofacies

Barrie (1999) described a peridotitic cumulate unit in the footwall to the Kidd Creek deposit that is similar to the coarse-grained ultramafic unit of the NR. Geochemically the two units contain similar amounts of MgO, the coarse-grained ultramafic unit of the NR has MgO values ranging from 23.5 to 33.7 wt% (Table 1) whereas the peridotite cumulate unit contains 20.1 to 31.5 wt% MgO (Barrie, 1999). The peridotite cumulate is characterized by a low rare earth element (REE) abundance with chondrite normalized values from 3 to 5, and by relatively flat REE patterns (Barrie, 1999). The coarse-grained ultramafic unit of the NR contains an overall lower abundance of REE's ranging from less than 1 to 3 × chondrite and REE patterns that are relatively flat except for a distinct positive or negative europium anomaly (Fig. 10a) that may indicate slight contamination from rhyolites locally intercalated with the ultramafic rocks, or hydrothermal alteration.

A fine-grained komatiitic unit described by Barrie (1999) is similar, petrographically, to the fine-grained komatiitic unit of the NR. The komatiites of the NR contain 23.8 to 33.5 wt% MgO (Table 1), therefore are more Mg-rich than those komatiites of the Kidd Creek footwall, which contain 17.7 to 24.0 wt% MgO (Barrie, 1999). The Kidd Creek footwall komatiites have REE concentrations with chondrite normalized values ranging from 4 to 15 × chondrite with relatively flat patterns, whereas the NR komatiites have lower overall REE values ranging from < 1 to 3 × chondritic values, but with the same relatively flat REE patterns (Fig. 10b).

The overall lower REE abundance in the coarse-grained ultramafic rocks and in the komatiitic flows of the NR are interpreted to be the result of a more olivine-rich ultramafic rock supported by their higher MgO content compared to the footwall ultramafic rocks at the mine. The higher MgO content of the ultramafic rocks of the NR indicates that they are more primitive than those of the Kidd Creek footwall and their more dunitic composition suggests that they may be the product of a proximal, sheet flow facies as opposed to the channel flow facies proposed by Barrie (1999) for the Kidd Creek footwall komatiites.

A gradational contact between the coarse-grained massive ultramafic unit and the fine-grained ultramafic unit suggests the coarse-grained ultramafic unit is the coarser grained base of an ultramafic flow. Facing directions, determined by the asymmetric distribution of

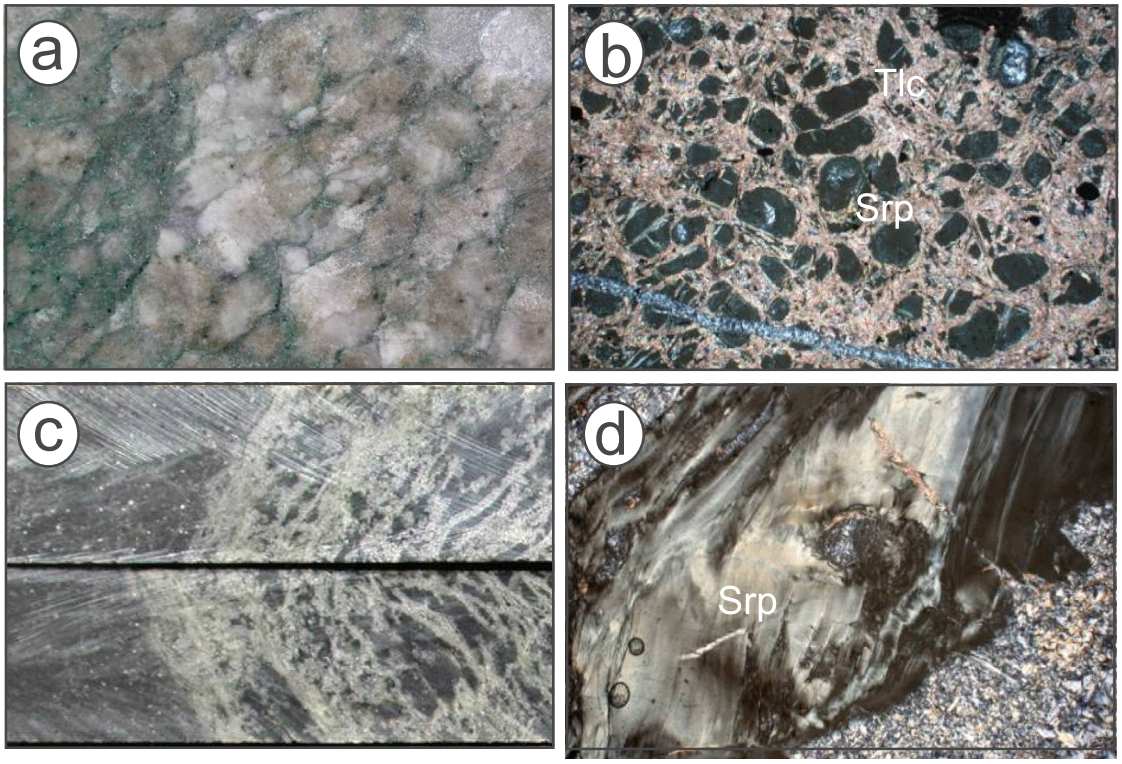

Fig. 5. Photographs and photomicrographs of the ultramafic units of the NR. Abbreviations are as follows: PPL plane polarized light; XPL cross-polarized light; DDH diamond drill hole. Mineral abbreviations after Kretz (1983). (a) Photograph of coarse-grained ultramafic unit (DDH 8495, 1540 m). (b) Photomicrograph (PPL) of serpentine after olivine preserving cumulate texture in the ultramafic rock from (a). The groundmass has been completely replaced by talc and carbonate. (c) Photograph of a flow top breccia of a fine-grained komatiitic unit. Arrow shows younging direction (DDH 4507, 548 m). (d) Photomicrograph (XPL) of a fracture from the komatiite flow top breccia in (c) filled with coarse-grained serpentine and rimmed with fine-grained serpentine.

polygonal flow top breccias and hyaloclastite within the komatiitic flow units, indicate that they occur stratigraphically below the rhyolites.

7.2. Aphyric rhyolite lithofacies

The aphyric rhyolites of the NR can however be separated, based on Al_2O_3 and TiO_2 ratios, from the QP rhyolites of the NR, and are compositionally identical to the aphyric rhyolites of the mine stratigraphy (Fig. 11a–c). The change from massive to in situ breccia to breccia facies within the aphyric rhyolite is gradational and is consistent with a change from the coherent interior of a flow or dome to its brecciated margin (e.g., Rutten, 1963; Wachendorf, 1973; Manley and Fink, 1987; Gibson, 1990; McPhie et al., 1993).

The contact between the rhyolite and the overlying mafic volcaniclastic unit is conformable as it is defined by a 1–2 m thick interval of mixed rhyolite (50%) and basalt (50%) clasts. The rhyolite blocks are interpreted to have been picked up and incorporated into mafic volcaniclastic debris flows as they moved over the blocky and brecciated surface of the underlying rhyolite. Where the mafic volcaniclastic unit is not present, aphyric rhyolite is conformably overlain by massive basaltic flows. The lower 10 m of the basal basalt flow seldom contains blocks of aphyric rhyolite that, like the mafic volcaniclastic unit, are interpreted to have been incorporated into the basalt flow as it travelled over the brecciated surface of the aphyric rhyolite.

7.3. Felsic volcaniclastic lithofacies

The homogeneity and single clast type in this unit indicates a proximal, single, aphyric rhyolite provenance. This lithofacies is similar in terms of clast type, texture and geochemistry to the felsic volcaniclastic unit that hosts the mineralization at Kidd Creek. It likely had a high primary permeability, which would have facilitated fluid movement laterally and vertically within the section. A significant portion of the Kidd Creek orebodies are interpreted to be a product of subseafloor replacement of aphyric, felsic volcaniclastic rocks (Hannington et al., 1999b).

7.4. Heterolithic volcaniclastic lithofacies

The occurrence of mafic clast types within the heterolithic volcaniclastic lithofacies indicates input of material from sources other than a proximal aphyric rhyolite dome or flow. As the NR shows no intercalation of aphyric rhyolite domes or flows and basalt flows, or monolithic basalt volcaniclastic rocks, it is unlikely that the basalt clasts found in the heterolithic volcaniclastic lithofacies are locally derived. There is no evidence for basaltic volcanism before or during the emplacement of aphyric rhyolite flows, domes and associated rhyolitic volcaniclastic rocks. Within the Kidd Creek mine strata, Prior (1996) describes mafic fragments within aphyric, rhyolitic volcaniclastic rocks where they are interpreted to be accidental clasts and occur in only trace amounts.

Any model to explain the occurrence of mafic clasts in the NR heterolithic volcaniclastic lithofacies must also explain why volcaniclastic rocks containing mafic fragments are intercalated with monolithic, aphyric rhyolite volcaniclastic rocks. One possible interpretation for their source and the intercalation of felsic monolithic and heterolithic volcaniclastic units is shown in Fig. 12. Here the intermittent collapse of aphyric rhyolite domes during their growth within a synvolcanic subsidence structure accounts for the deposition of felsic volcaniclastic units. This process combined with episodic faulting along the wall of the subsidence structure providing the input of mafic material derived from basalt flows outside of, or in the walls of, the subsidence structure is interpreted to result in the intercalation of heterolithic and felsic volcaniclastic rocks. The heterolithic volcaniclastic

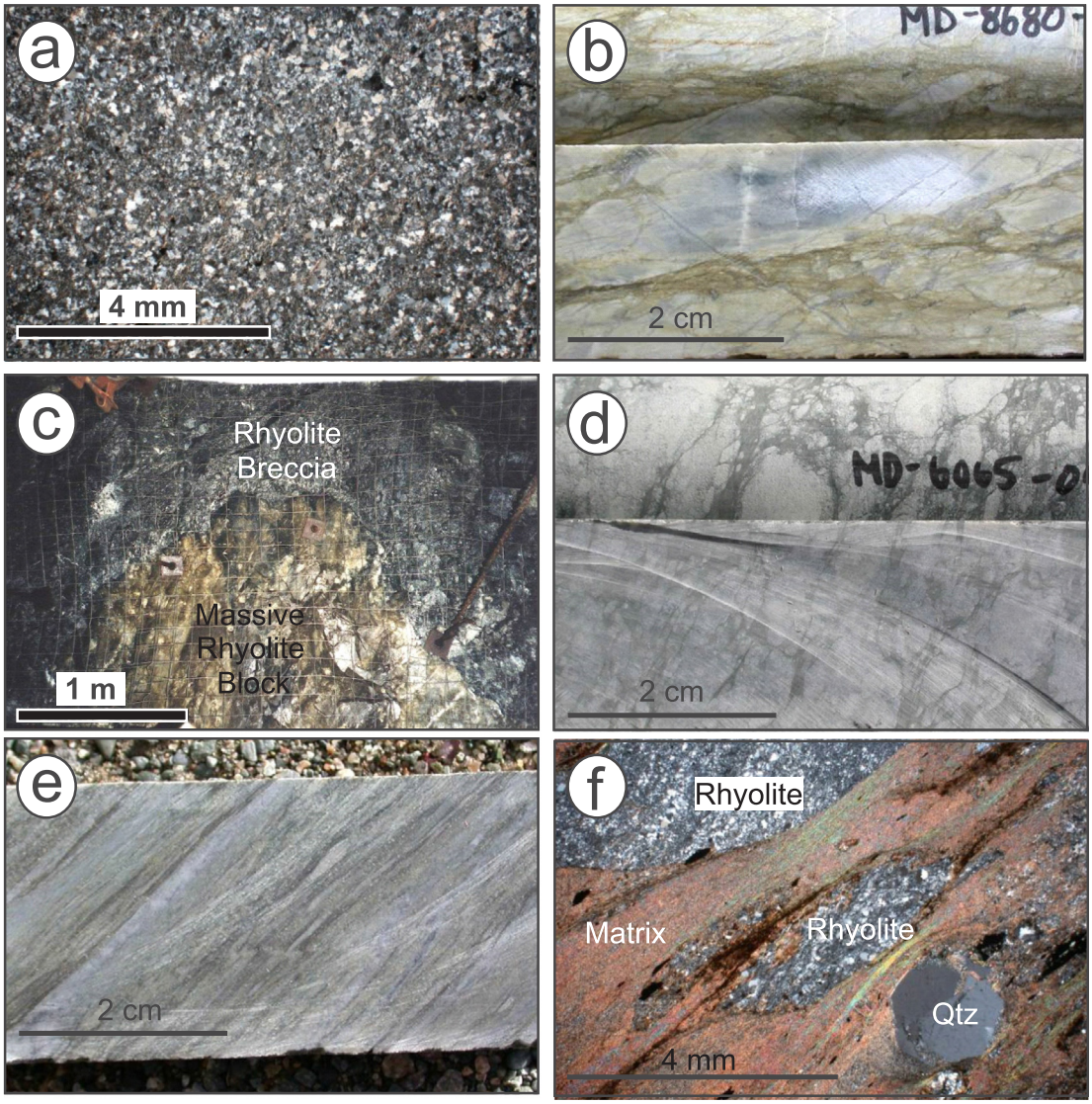

Fig. 6. Photographs and photomicrographs of rhyolitic units of the NR. (a) Photomicrograph (XPL) of massive, aphyric rhyolite (DDH 8495, 1498 m). (b) Photograph of in situ aphyric rhyolite breccia (DDH 8680, 560 m). (c) Photograph of block of flow banded, strongly sericitized aphyric rhyolite block in finer aphyric rhyolite breccia with strongly chloritized matrix, from 2800 L exploration drift. (d) Photograph of aphyric rhyolite breccia (DDH 6065, 513 m). (e) Photograph of rhyolite lapilli-tuff (DDH 4507, 733 m). (f) Photomicrograph (XPL) of a rhyolite lapilli-tuff from (e) containing a quartz crystal and rhyolite clasts in a strongly sericitized matrix. Abbreviations as in Fig. 4.

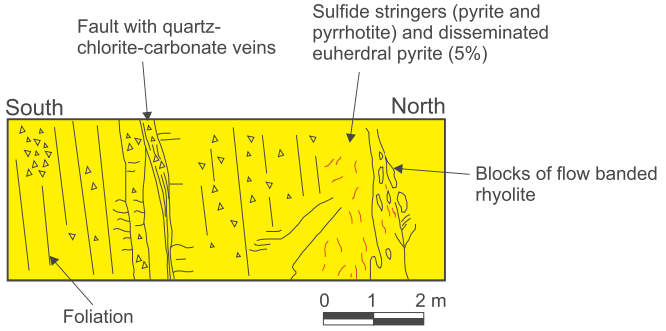

Fig. 7. Wall map drawn from 2800 Level exploration drift exposure, showing brecciated to massive, strongly foliated rhyolite with sulfide mineralization. Younging is to the right. See Fig. A.1 for location within drift.

units also contain angular clasts of massive pyrite and sphalerite, indicating that seafloor VMS mineralization occurred either with the aphyric rhyolite flows or domes that provided the rhyolitic clasts, or along the synvolcanic faults that are interpreted to have provided the mafic clasts and may have exposed older sulfide mineralization as well.

7.5. QP rhyolite lithofacies

Gradational changes within the QP rhyolite from coherent to brecciated facies is consistent with a change from the coherent interior of a flow or dome to its brecciated margin, as was the case for the aphyric rhyolite. The gradational upper contact of the QP rhyolite with the mafic volcaniclastic lithofacies, or the basalt where the mafic volcaniclastic lithofacies is absent, including the occurrence of rhyolite clasts within the overlying mafic lithofacies, suggests the rhyolite clasts were incorporated into the mafic volcaniclastic lithofacies and basal portion of the basalt flows as they travelled over the QP rhyolite.

The QP rhyolite is distinct petrographically and geochemically from the aphyric rhyolite unit and can be separated not only based on its phenocrysts content, but also its Al_2O_3 and TiO_2 ratios (Fig. 11a, b). Also, when compared to the QP rhyolite of the mine stratigraphy, the QP rhyolite of the NR displays nearly identical REE patterns (Fig. 11c).

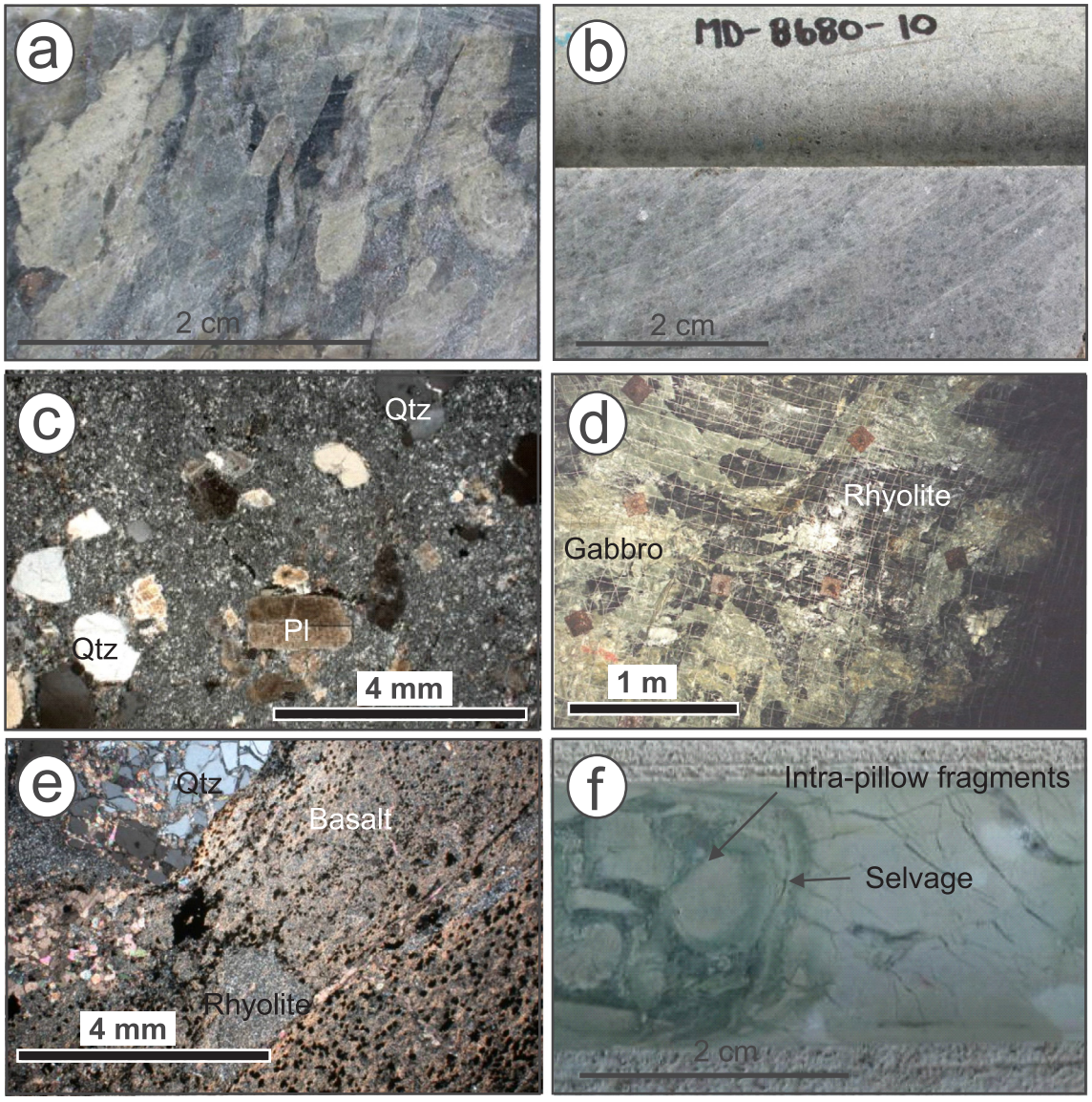

Fig. 8. Photographs and photomicrographs of rhyolitic units of the NR. (a) Photograph of heterolithic volcaniclastic unit (DDH 8697, 343 m). (b) Photograph of massive QP rhyolite (DDH 8680, 239 m). (c) Photomicrograph (XPL) of QP rhyolite from (b). (d) Photograph of peperite from 2800 Level exploration drift. (e) Photomicrograph (XPL) of mafic volcaniclastic unit showing amygdaloidal basalt clast, aphyric rhyolite clast, and fractured quartz crystal in very fine grained quartz, carbonate, sericite matrix. (f) Photograph of basaltic pillow breccia (DDH 2104, 170 m). Abbreviations as in Fig. 4.

The NR and Kidd Creek mine rhyolites (both QP and aphyric) have REE patterns similar to FIIIb rhyolites of the Superior Province (Fig. 11c; Lesher et al., 1986).

Given that rhyolite volcanism in the Kidd Mine and NR areas is centred on 2716 Ma and that at most the QP and aphyric rhyolite are separated by 2 million years at most (Bleeker and van Breeman, 2011), but probably much less (accounting for error of U-Pb zircon ages), it is likely that that compositional difference between the QP and aphyric rhyolites of the NR is likely a product of fractionation from a single source magma as has been suggested for the Kidd Mine rhyolites (Bleeker and van Breeman, 2011). Both the aphyric and QP rhyolite units in the main mine sequence are interpreted to be the products of partial melting of hydrated mafic volcanic rocks in a high heat flow environment, which is interpreted to have driven the mineralizing hydrothermal system at Kidd Creek (Prior et al., 1999a–c). The ε_{Nd} values from the Kidd Creek mine rhyolites range from 1.1 to 4.2, which are similar to those collected elsewhere in the Superior Province and are consistent with the Kidd Creek orebodies forming in an ensimatic environment, possibly a mid-ocean rift, well away from continental margins (Prior et al., 1999b). Lead and neodymium isotope work done by Barrie et al. (1999) also reflects a direct derivation from a primitive (Pb) or depleted MORB-like (Sm-Nd) mantle, with little or no influence from older crustal components.

7.6. Argillite lithofacies

The occurrence of argillite units is indicative of periods of volcanic quiescence, dominated by suspension sedimentation, between mass debris flows that were derived from the collapse of, or faulting near, rhyolitic flows/domes, or eruptions of basalt.

7.7. Peperite lithofacies

Peperite occurs at the contact between aphyric rhyolite volcaniclastic lithofacies and overlying basalt and may have formed: (1) through the intrusion of mafic sills into wet unconsolidated rhyolitic volcaniclastic material; or (2) through invasive basaltic flows that settled into unconsolidated volcaniclastic rocks (Beresford and Cas, 2001).

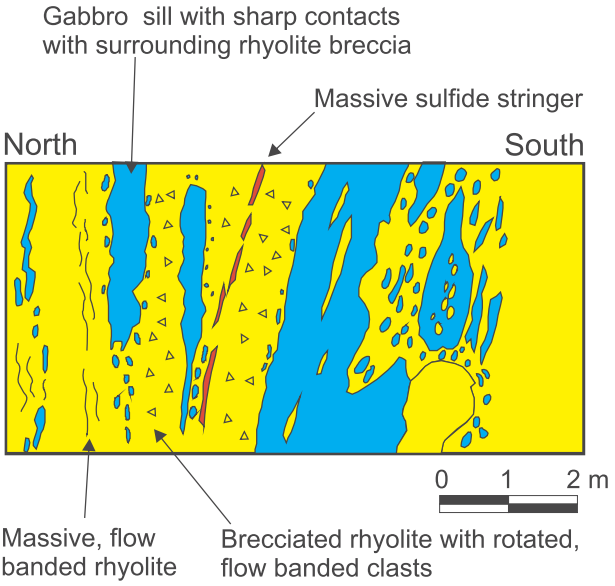

Fig. 9. Wall map drawn from 2800 Level exploration drift exposure, showing complex relationship between rhyolite breccia and mafic sills forming a peperite. Youning is to the left. See Fig. A.1 for location within drift.

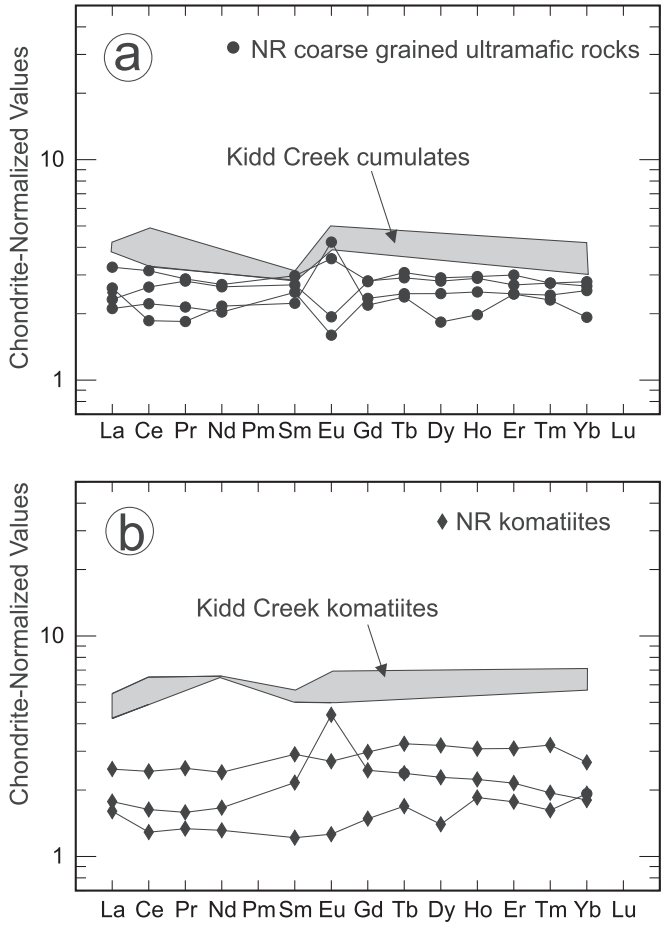

Fig. 10. REE plots for ultramafic rocks of the NR compared with ultramafic footwall rocks of the Kidd deposit (Barrie, 1999), normalized to the chondritic values of Sun and McDonough (1989).

Both mechanisms may have been involved in the formation of peperite within the NR. However, close spatial association between mafic sills and peperite, and commonly gradational contacts between the sills

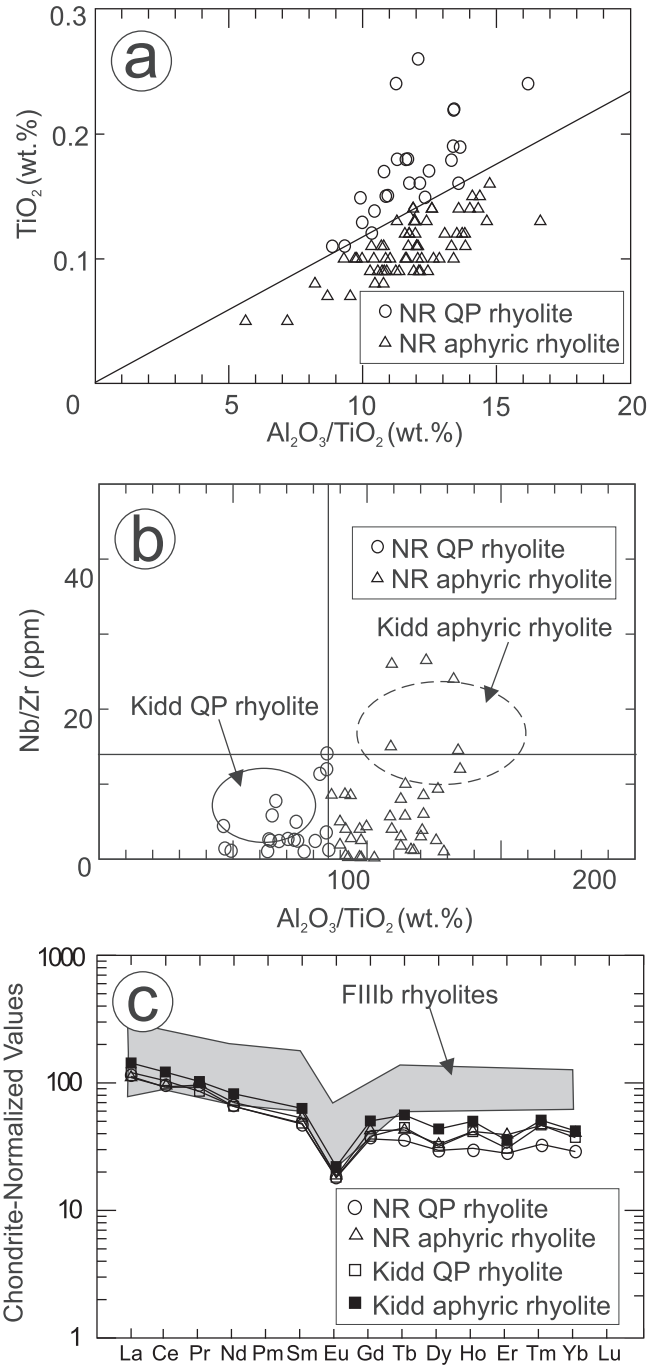

Fig. 11. Al_2O_3/TiO_2 vs. TiO_2 (a) and Nb/Zr (b) diagrams that discriminate the QP and aphyric rhyolites of the NR and compare them to the Kidd Creek mine QP and aphyric rhyolites (Prior et al., 1999a). (c) Comparison of chondrite-normalized REE patterns of FIIIb rhyolites (grey field; Lesher et al., 1986) of the Superior Province, and average NR and Kidd mine rhyolites. Chondrite-normalizing values are those of Nakamura (1974).

and peperite, suggest that the peperite within the NR strata likely formed because of the intrusion of mafic magma into wet unconsolidated rhyolite volcaniclastic deposits. Peperite occurring at the contact between the basalt and underlying rhyolite volcaniclastic rocks may have formed where the basalt flows moved over and locally burrowed into unconsolidated rhyolitic volcaniclastic deposits on the seafloor. As within the Kidd Creek mine strata, the mafic sills are much thicker (an average of 28 times thicker) and more abundant on the southwest limb of the NR fold than on the northern limb, suggesting the

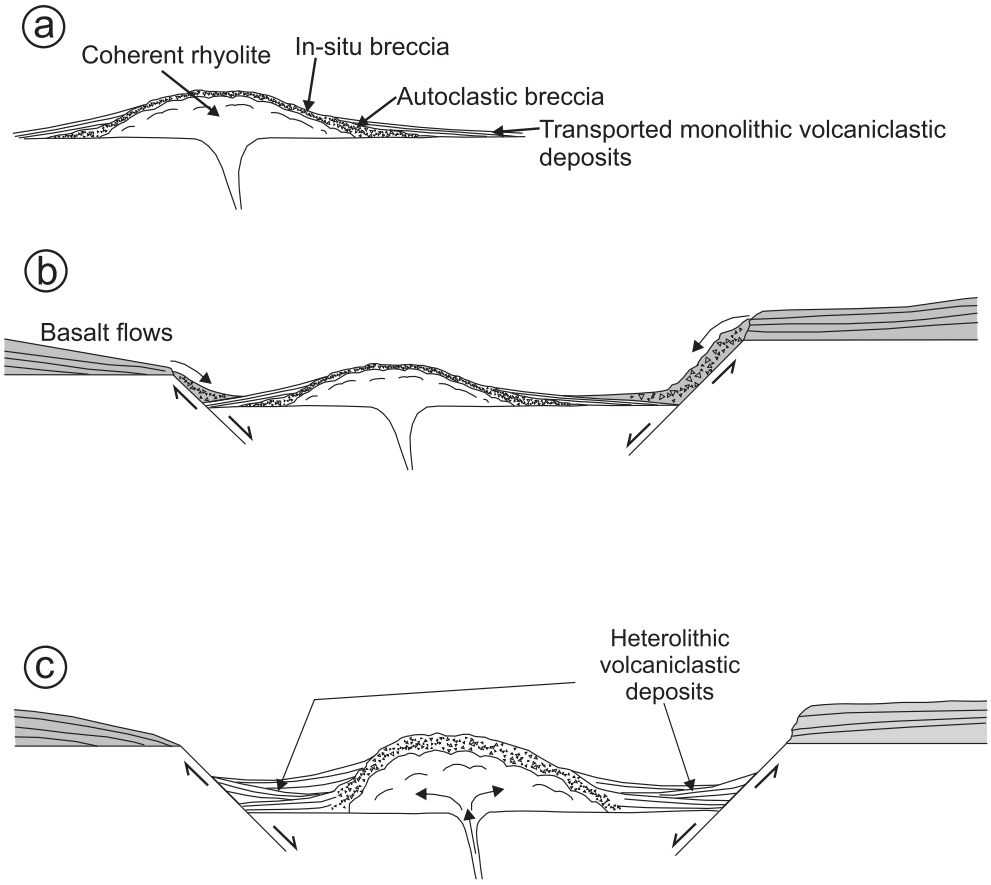

Fig. 12. Conceptual model to explain the emplacement of monolithic (felsic) and heterolithic volcaniclastic rocks. (a) The emplacement of a rhyolite dome and associated monolithic breccia and finer volcaniclastic facies. (b) Subsequent down faulting and mixing of basalt clasts from lava flows located outside of the immediate subsidence structure (minor) with rhyolite clasts forming heterolithic volcaniclastic deposits. (c) The continued growth of the rhyolite dome causes the generation and deposition of more monolithic volcaniclastic debris on top of the heterolithic volcaniclastic deposits. Not to scale.

southwest limb, which also contains the Kidd Creek mine, represents a more vent proximal volcanic area.

7.8. Mafic volcaniclastic lithofacies

The variable clast size, abundance, and sorting suggest that the mafic volcaniclastic lithofacies were deposited by various debris flows. As the mafic volcaniclastic lithofacies mainly consists of basalt (60%) and rhyolite (15%) clasts in a mafic tuff matrix, but there is no intercalation of rhyolite and basalt within the NR or Kidd Creek mine strata, it is likely that the mafic component of the mafic volcaniclastic unit came from outside the immediate NR and Kidd Creek mine areas. Subsidence associated with the emplacement of rhyolite domes in the area of the NR is interpreted to have exposed distal basaltic flows along fault scarps. Mass debris flows generated by collapse along these faults scarps then travelled down slope, picking up rhyolite clasts as they travelled over rhyolite domes. Subsequent subsidence and faulting associated with basaltic volcanism in the area of the NR resulted in the unroofing of the rhyolite domes, triggering mass flows comprising mafic and rhyolitic clasts, which were deposited on top of basalt flows, accounting for the presence of mafic volcaniclastic beds between basaltic flows in the hanging-wall (Fig. 13).

7.9. Basalt lithofacies

Bleeker (1994) subdivided the hanging-wall to the Kidd Creek deposit into: (1) a basal package of low TiO_2 basalts ($TiO_2 \leq 1.0$ wt%); a middle package of high TiO_2 basalts (TiO_2 typically > 1.5 wt%); and an upper package of low TiO_2 basalts (TiO_2 ca. 1 wt%). Wyman et al. (1999) confirmed this subdivision and classified the three packages as a lower zone of both MORB-type and arc-like tholeiites, a middle zone of primitive arc tholeiites, and an upper zone of evolved arc tholeiites. The basalt of the NR is divisible into two distinct units based on weight percent TiO_2 and P_2O_5: low Ti and P flows (0.10–1.55 wt% TiO_2, 0–0.27 wt% P_2O_5) and high Ti and P flows (> 1.55 wt% TiO_2 and > 0.27 wt% P_2O_5; Fig. 14). The low TiO_2 basalt flows directly overlie the QP rhyolite and are, in turn, overlain by the high TiO_2 flows. Low and high TiO_2 basalts are continuous along both limbs of the NR fold. There is no tuff or sediment present between the two chemically distinct basaltic units and thus no obvious time gap. We interpret the low TiO_2 flows of the NR to correspond with Bleeker's lowermost package of low TiO_2 basalts, the high TiO_2 basalts of the NR to correspond with the middle package of high TiO_2 basalts and that the drill holes that penetrated the NR were not long enough to intersect the uppermost package of low TiO_2 basaltic flows. The low and high TiO_2 basalt units may be the product of one continuous eruption, or of multiple eruptions.

Only samples from the lowest basalt flow with the NR stratigraphy were analyzed for trace elements. Based on Zr-Th-Nb and Ti vs V systematics these basalts are similar to mid-ocean ridge basalts (MORB) and correspond with the MORB-like basalts that occur immediately above the QP rhyolite in the Kidd Mine stratigraphy in what Wyman et al. (1999) called a "diverse zone of mafic flows" (Fig. 15a, b). Chondrite-normalized patterns for the lowermost basalt flows of the NR also match those of the MORB-like basalt flows that occur immediately above the QP rhyolite in the Kidd Mine stratigraphy (Fig. 15c) with relatively flat REE patterns.

Facing direction, indicated by pillow morphology and the asymmetric concentration of amygdules towards upper pillow margins, agree with the facing directions of the ultramafic flows and clearly define the NR anticline. The contact between the basalt flows and mafic volcaniclastic rocks is conformable as evidenced by amoeboid clasts of mafic volcaniclastic rock in the overlying basalt. The voluminous package of hanging-wall basalts marks the end of rhyolite volcanism

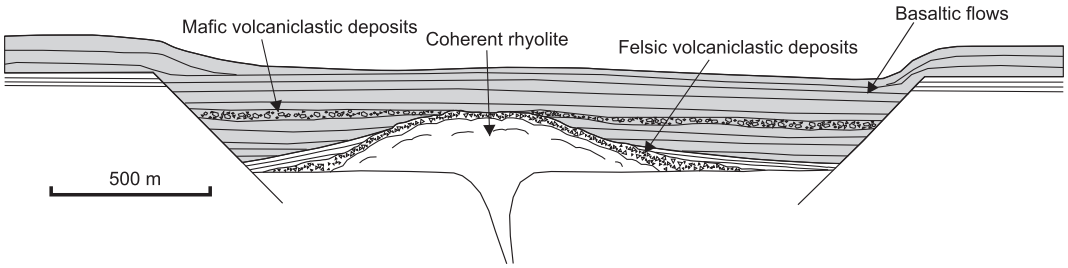

Fig. 13. An explanation for the presence of bedded mafic volcaniclastic rocks between massive basalt flows. In this interpretation basalt flows begin to cover the underlying rhyolite topography. Collapse along fault scarps results in the deposition of mafic volcaniclastic debris, which contains rhyolite clasts that are picked-up as mass flows traveled over underlying rhyolite volcaniclastic deposits. Subsequent emplacement of more basalt flows and the repetition of these events may explain the intercalated nature of the basaltic flows and mafic volcaniclastic units near the base of the hanging-wall basaltic succession.

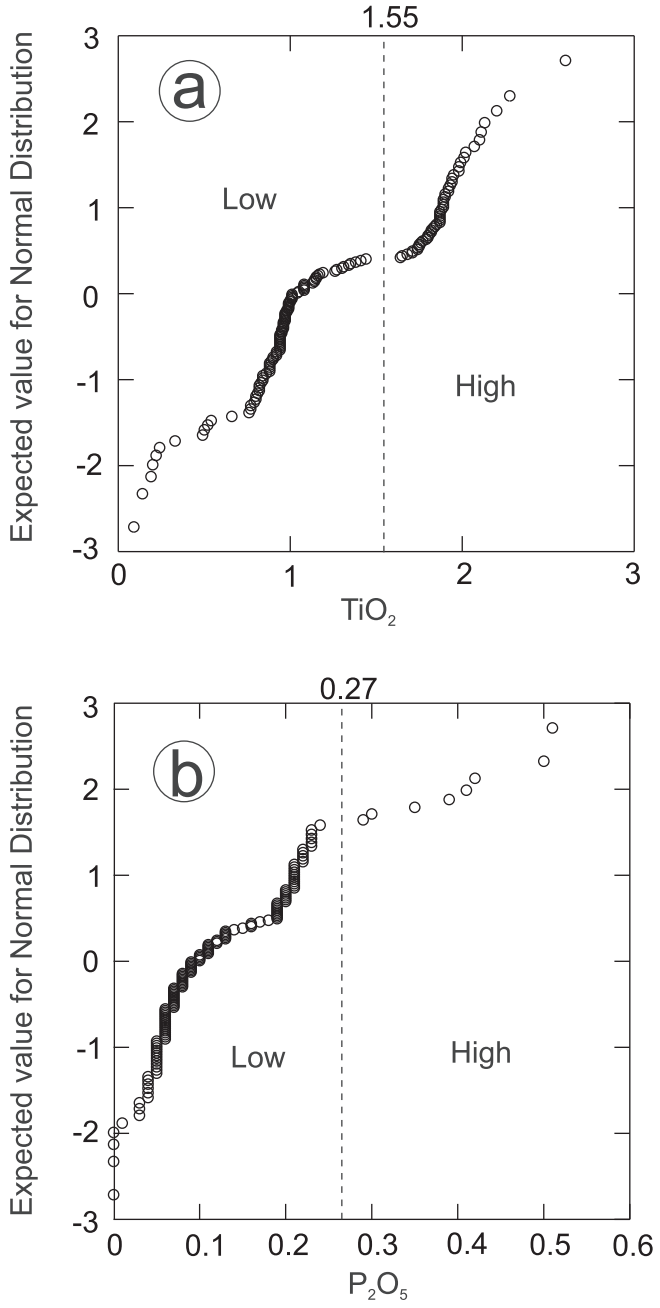

Fig. 14. Cumulative frequency curves showing the subdivision of basalt into two chemically distinct units based on TiO_2 and P_2O_5 values.

and hydrothermal activity within the NR, and their extensive lateral distribution indicates they were not restricted by underlying topography.

8. Volcanic reconstruction

8.1. Methodology

Using the contact between the basalt and rhyolite on both the northeastern and southwestern limbs of the F_1 NR anticline from over 150 drill holes, two surfaces were created in GoCAD representing the basalt – rhyolite contact on each limb of the NR anticline (Appendix D, Fig. D.1). The two limbs (and mine grid) were then rotated 60° about the point 64750E, 66000N so that they could be projected onto a flat plane. If the limbs were not rotated by 60°, the Hinge Zone (Figs. 2, 4) would be perpendicular to the projection plane and therefore not visible in two dimensions. The Hinge Zone (the northern most extension of the NR anticline) and the main part of the NR fold (interpreted to be the extension of the Kidd Creek Mine fold) then had to be rotated 35° to be parallel to the projection plane. Instead of rotating the Hinge Zone and the main part of the fold the points on the surfaces representing the north and south limbs were projected onto the flat projection plane and scaled by 22% from a central point of 64650E, 66000 N (Fig. D.2). The 22% scaling is from simple trigonometry where:

$$\cos 35 = 100\,\text{m}/X, \text{ therefore } X = 122\,\text{m}$$

Thus, the paleo-seafloor lengths are 22% longer from the center point. The new flat surface represents an approximation of the paleo-seafloor post rhyolite volcanism. All of the drill hole pierce points for the northeast and southwest limbs were transformed from mine coordinates to pre-deformational paleo-seafloor coordinates using the equation shown in Table D.1.

The pierce points of 50 drill holes that intersected the basalt-rhyolite contact on both limbs of the NR fold were also rotated such that they define data-location points on the NR paleosurface. These intersection points were used to contour rhyolite thickness data, as well as alteration indices on the paleosurface (Figs. 16, 17).

Stretching or shortening of the NR has not been corrected because all the units occur on the limbs of the NR anticline. Thickening due to folding would have occurred primarily in the F_1 fold nose and only data from the limbs of the fold are used. Axial planar parallel, sinistral faults that offset the Kidd Creek orebodies are also recognized in the NR (Fig. 2); however, as in the Kidd Creek area, these faults have not caused significant offset and therefore have not significantly affected rhyolite distribution and thickness.

Other assumptions used in the reconstruction include: (1) the low viscosity komatiitic flows that underlie the succession are assumed to have produced an essentially flat paleotopography, therefore the underlying komatiitic topography did not affect the rhyolite topography, and (2) coherent rhyolite domes and flows created positive topographic features on the flat komatiitic flows. If these assumptions are valid,

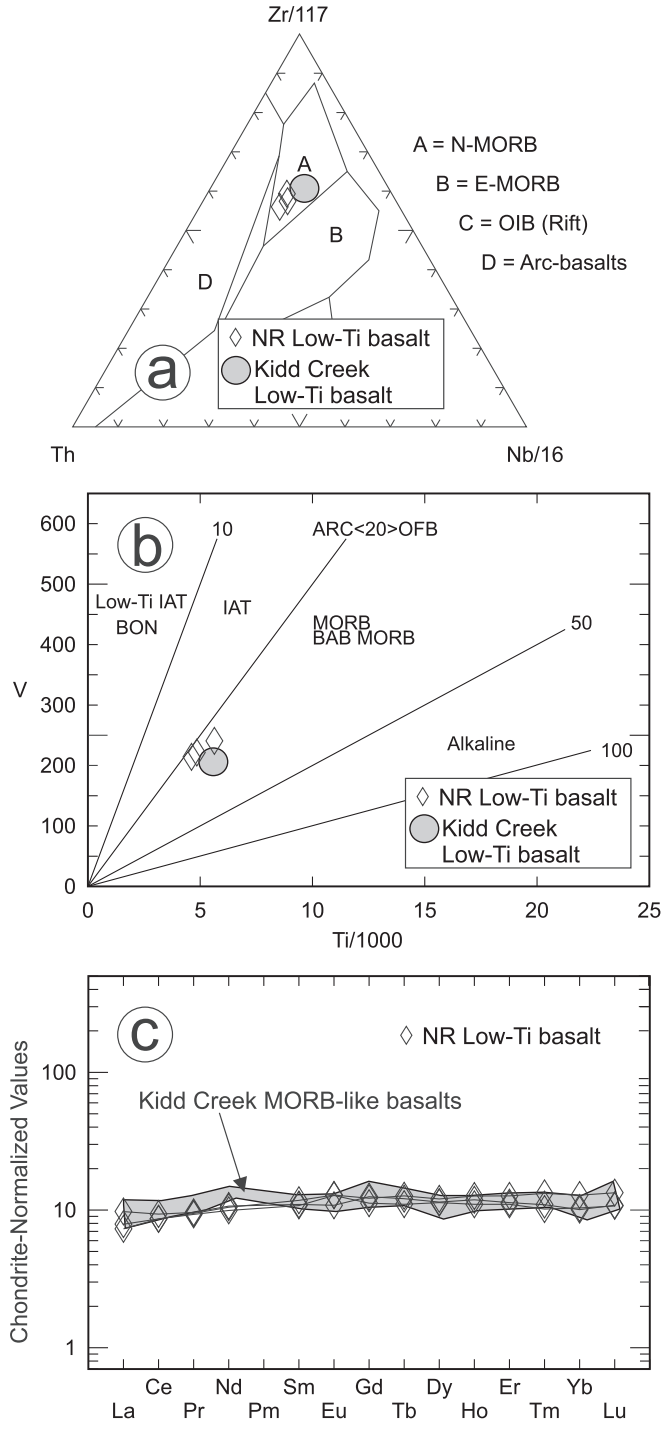

Fig. 15. Figures comparing the geochemistry of the basal basalt flows of the NR to those of the Kidd stratigraphy (Wyman et al., 1999). (a) Zr-Th-Nb tectonomagmatic discrimination diagram (Wood, 1980); (b) Ti-V tectonomagmatic discrimination diagram (Shervais, 1982); (c) chondrite-normalized trace element plots. Chondrite values from Sun and McDonough (1989).

areas of pronounced coherent rhyolite thickening can be interpreted as primary, thicker portions of the flows and domes rather than deformation-induced features, and the orientation of domes relative to each other, or their alignment, may indicate a primary structural control on their location and emplacement, and any associated alteration and mineralization.

8.2. Distribution of rhyolite

Fig. 16a contains rhyolite isopach maps showing a reconstruction of the NR aphyric rhyolite domes on the paleo-seafloor. Note that in Fig. 16 the fold axis represents a northwest orientation. Coherent, aphyric rhyolite typically occurs as east northeast-trending ridges that are 15 to 80 m high, and 500 to 1500 m long. The exception to orientation is an approximately west-northwest-trending, 1 km long by 28 to 80 m high aphyric rhyolite ridge, which may in fact be two separate domes (Fig. 16a). On the southwest limb of the anticline the thickest aphyric rhyolite (35 m) occurs north to northwest of, and parallel to, the adjacent Kidd Creek orebodies that overly a massive aphyric rhyolite ridge extending the full length of the orebodies (Prior, 1996; Prior et al., 1999a). The northwestern portion of the southeast limb contains one small dome of massive aphyric rhyolite (Fig. 16a). Aphyric rhyolite in situ breccia directly overlies, or is adjacent to, the coherent rhyolite flows/domes and ranges in thickness from 5 to 134 m (Fig. 16a).

Fig. 17a contains rhyolite isopach maps showing a reconstruction of the NR QP rhyolite domes on the paleo-seafloor. Thickness variations in coherent QP rhyolite define ridges that are 65 to 113 m high, 300 to 2000 m long and trend east-northeast; an east–west trend is less pronounced (Fig. 17a). The thickness and east-northeast orientation of the QP rhyolite is the same as the QP rhyolite that overlies the Kidd Creek orebodies (Prior et al., 1999a). Overall, the ratio of QP rhyolite in situ breccia to massive QP rhyolite (1:3.4) is much lower than the ratio of aphyric rhyolite in situ breccia to massive aphyric rhyolite (1:4.7). QP rhyolite in situ breccia ranges in thickness from 4 to 66 m and directly overlies or is adjacent to coherent QP rhyolite domes and flows (Fig. 17a).

8.2.1. Interpretation of rhyolite

The uniform rhyolite clast composition and distribution of the volcaniclastic facies, for both the aphyric and QP rhyolites, relative to their massive, coherent facies indicates that the volcaniclastic facies represents material derived from the collapse, or over-steepening of rhyolite domes, with the debris subsequently re-deposited by mass flows into proximal topographic lows or basins. The in situ breccias located directly on top, and on the flanks, of the massive domes and flows represent the autobrecciation of the margins of the domes and flows, as they show no evidence of transportation (i.e. bedding, rotated clasts, round clasts). By comparison the volcaniclastic facies adjacent to the coherent rhyolite locally contain evidence of transportation such as crude bedding, rotated clasts and round clasts.

The aphyric rhyolite volcaniclastic facies of the southwest limb is interpreted to represent autoclastic rhyolite breccia that has been shed from the massive aphyric rhyolite ridge that lies stratigraphically below the Kidd Creek orebodies (Fig. 16a). The northeast limb of the NR fold is almost entirely blanketed by coherent or volcaniclastic facies of aphyric rhyolite including a 20 to 50 m high massive aphyric rhyolite ridge in the northeast that may increase in size outside the study area.

Massive aphyric rhyolite domes of the NR are generally controlled by two linear east northeast-trending structures interpreted to represent fissures through which the rhyolite was extruded. The west-northwest-trend of a single rhyolite ridge on the northeast limb of the anticline is poorly delineated due to sparse drill hole data and may represent two separate domes. This rhyolite ridge orientation within the NR is the similar to as the northwest-trending structure that is inferred to have controlled the distribution of bornite mineralization in the Kidd Creek South Ore Body where it is referred to as the bornite trend (Hannington et al., 1999a; Bleeker, 1999). The dominant east-northeast-trend of the NR aphyric rhyolite is the same as the trend of the massive aphyric rhyolite ridge that underlies the Kidd Creek orebodies (Fig. 13a; Bleeker, 1999, Prior et al., 1999a), indicating significant structural control on the emplacement of the aphyric rhyolite extending to the area of the NR from the immediate area surrounding the Kidd Creek

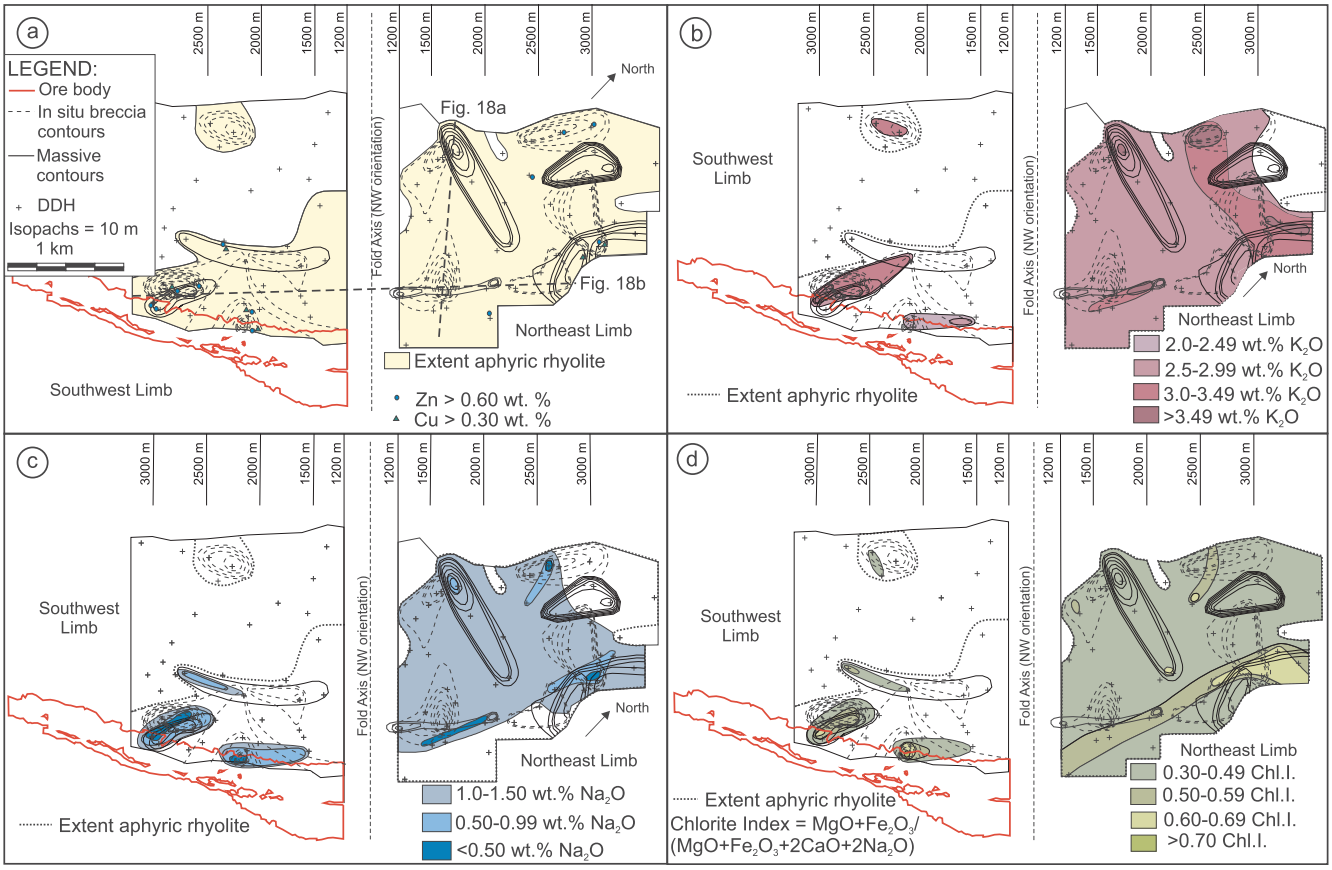

Fig. 16. Isopach maps showing the distribution of massive and brecciated facies of the aphyric rhyolite unit as well as: (a) extent of aphyric rhyolite including all aphyric rhyolitic volcaniclastic rocks, (b) potassium alteration – avg. K_2O wt% over the entire intersected interval within each drill hole, (c) sodium alteration – Na_2O wt% over the entire intersected interval within each drill hole, (d) chlorite index. Note: For figures b-d, non-shaded areas within extent of rhyolite means < 2.0 K_2O wt%, > 1.50 Na_2O wt% and a chlorite index of < 0.30 respectively. DDH = diamond drill hole. Meter markers reflect meters below surface.

deposit. The minimum volume of massive coherent aphyric rhyolite is estimated at 0.06 km^3 and coherent plus in situ brecciated aphyric rhyolite has an estimated volume of 0.13 km^3.

The distribution of coherent QP rhyolite shows a more pronounced structural control as it occurs as two linear ridges that trend east-northeast and are interpreted to overlie fissures through which the rhyolite domes were extruded. The similarity between the orientation of the QP rhyolite domes within the NR to those defined for the Kidd Creek QP rhyolite domes (Prior et al., 1999a) indicates that the emplacement of the QP rhyolite was controlled by structures with the same orientation over a larger area than was previously known. The massive coherent QP rhyolite of the NR has an approximate volume of 0.05 km^3 with a minor amount of in situ breccia estimated at 0.01 km^3.

The more restricted areal extent and pronounced structural control of the QP rhyolite may relate to a higher viscosity for this unit as compared to the compositionally similar aphyric rhyolite. To test this hypothesis the viscosity of the aphyric and QP rhyolites were calculated using the using the model of Giordano et al. (2008), the whole rock geochemistry of the aphyric and QP rhyolites, and their calculated eruption temperatures of 960 °C (Barrie, 1995). The calculation indicates that for varying degrees of dissolved water content (0–5%) the effective viscosities for the aphyric and the QP rhyolite are within 0.20 Pa s for each hypothetical dissolved water content (Table 2). Because the effective viscosities are so similar we interpret the QP rhyolite domes to have been emplaced with lower effusion rates, potentially coupled with lower eruption temperatures, resulting in the more restricted areal extent of the QP rhyolite, and the smaller volume of associated volcaniclastic facies.

The continuous occurrence of both the aphyric and QP rhyolite from the Kidd Creek mine area to the NR indicates that the rhyolite field is much larger than previously proposed. Aphyric and QP rhyolite, correlative with those units in the Kidd Creek mine area, occur on both limbs of the NR fold and are therefore not completely restricted by a major synvolcanic fault just north of the Kidd Creek orebodies (Bleeker, 1999). Figs. 16 and 17 show that both the aphyric and QP are present on both sides of the fold axis and that neither unit shows a drastic change in thickness or facies variations across the fold axis.

Fig. 18a and b are two cross sections (locations of cross-sections shown on Fig. 16a) constructed through the NR to illustrate the size and shape of the aphyric rhyolite. Fig. 18a depicts two aphyric rhyolite domes, one dominated by massive rhyolite and the other dominated by autoclastic breccia, the latter of which is interpreted to represent the brecciated carapace on, or adjacent to, a coherent rhyolite dome (i.e., the coherent portion of the dome was not intersected by drill holes, so it is not portrayed on Fig. 16a). The cross-section in Fig. 18b shows two coherent rhyolite domes blanketed by autoclastic breccia as is typical of subaqueous blocky rhyolite flows and domes (McPhie et al., 1993; Gibson et al., 1999), and a coherent rhyolite dome with an adjacent 80 m high autoclastic breccia facies that is interpreted to represent the margin of another coherent rhyolite dome located off this section.

Fig. 19a and b are cross-sections through the QP rhyolite ridges. The QP rhyolite domes have a more limited areal extent and consist almost entirely of massive rhyolite with only minor amounts of autoclastic breccia, a characteristic that is interpreted to be a result of a higher viscosity and lower effusion rate for the QP rhyolite compared to the aphyric rhyolite.

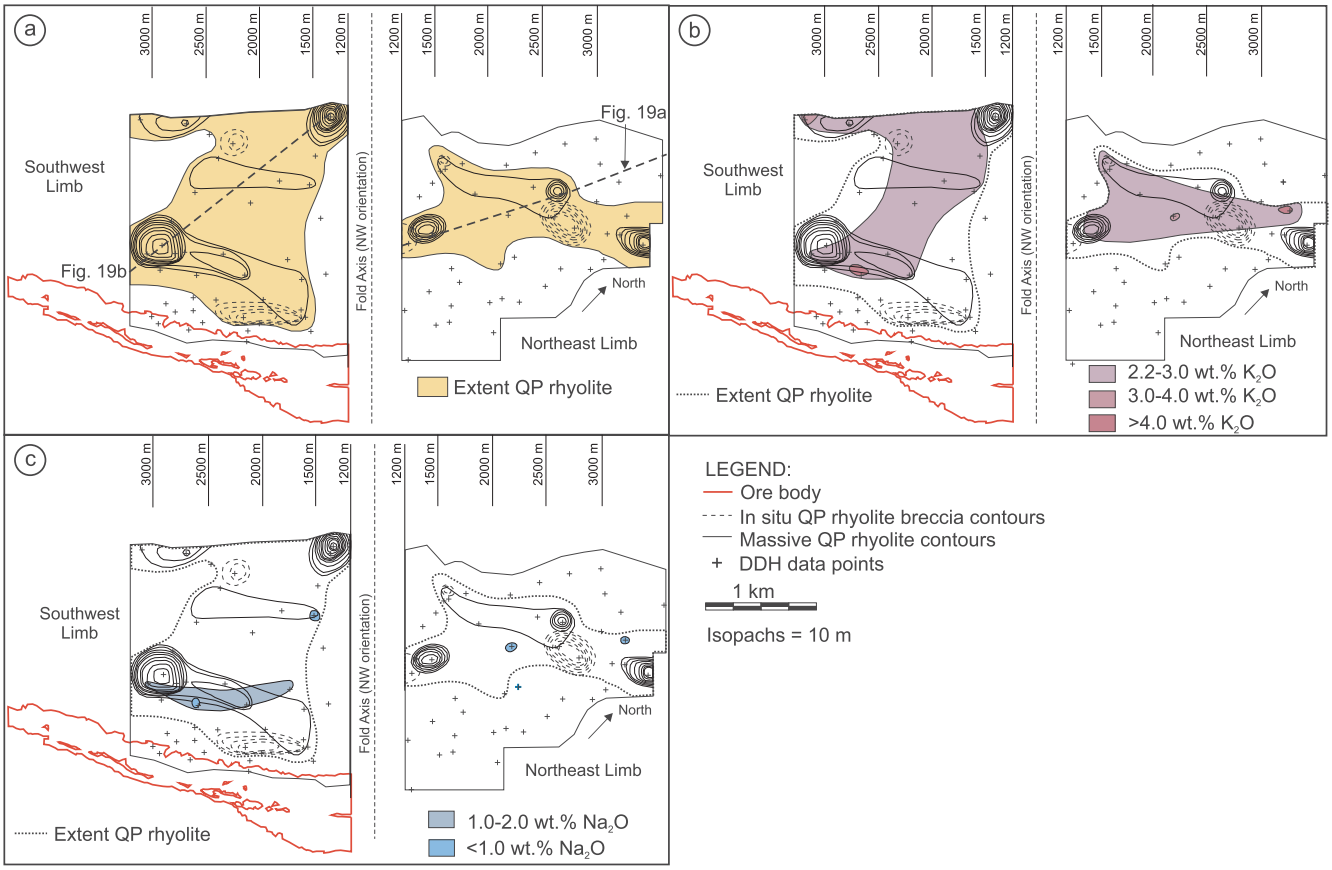

Fig. 17. Isopach maps showing the distribution of massive and brecciated facies of the QP rhyolite unit as well as: (a) extent of QP rhyolite including all QP rhyolitic volcaniclastic rocks, (b) potassium alteration – avg. K_2O wt% over the entire intersected interval within each drill hole, (c) sodium alteration – Na_2O wt% over the entire intersected interval within each drill hole. Note: For figures b-c, non-shaded areas within extent of rhyolite means < 2.0 K_2O wt% and > 1.50 Na_2O wt% respectively. DDH = diamond drill hole. Meter markers reflect meters below surface.

Table 2
Effective viscosities for rhyolites of the NR based on hypothetical water contents and model of Giordano et al. (2008).

Aphyric Rhyolite		QP Rhyolite	
wt% H_2O	Viscosity (Pa s)	wt% H_2O	Viscosity (Pa s)
H_2O = 0	7.64	H_2O = 0	7.51
H_2O = 1	6.23	H_2O = 1	6.10
H_2O = 2	5.43	H_2O = 2	5.32
H_2O = 3	4.84	H_2O = 3	4.73
H_2O = 4	4.35	H_2O = 4	4.25
H_2O = 5	3.93	H_2O = 5	3.84

8.3. Distribution of basalt

The low TiO_2 basalt flows of the NR, which are correlative with those in the immediate hanging-wall for the Kidd Creek deposit (Bleeker, 1999; Wyman et al., 1999), are present in all drill holes where whole rock data is available, and lie directly above the QP rhyolite, or the aphyric rhyolite if the QP rhyolite is not present. The low TiO_2 basaltic flows of the NR range in thickness from 100 to 934 m and have an estimated minimum volume of 10.5 km^3. This estimate of volume is based on the average thickness for the unit calculated from the seven drill holes that intersected the overlying high TiO_2 flows. The high TiO_2 basalt covers the entire NR study area, except for a small area to the southeast where a large gabbroic sill occupies this stratigraphic position, though drilling in this area is limited. However, the low TiO_2 basaltic flows constitute only a small portion of the voluminous basalt sequence that overlies the Kidd Creek deposit and NR, extending east and west into the Kidd 66 and Kidd West basins. The total volume of this entire hanging-wall basaltic sequence is estimated to be on the order of 7000 km^3.

8.3.1. Interpretation of basalt

The basalt flows inundate the NR topography on both limbs of the NR anticline, such that the lowermost low TiO_2 basaltic flows buried all the aphyric and QP rhyolite domes, which are up to 113 m high. A large gabbroic sill in the southeast part of the reconstructed plan was intruded along the QP rhyolite-basalt contact and at the aphyric rhyolite-basalt contact, thereby displacing the basalt, which was subsequently eroded. Thus, the absence of basalt in this area does not indicate the absence of basalt volcanism entirely.

Although data are limited, the low TiO_2 basalt does not show systematic changes in thickness from one area to another. The thickness of the basalt appears only to depend on the thickness of the underlying rhyolite. Where the rhyolite is thinner the basalt is thicker and over larger rhyolite domes the basalt is thinner. However, with only seven drill holes intersecting the low TiO_2 flows, the interpretation of overall basalt thickness and distribution, with respect to the rhyolite domes, may be an artifact of insufficient data coverage. The extensive nature and area covered by the basaltic flows does; however, indicate that, that the graben wall interpreted north of the mine, did not restricted basalt flows from continuing to the north.

9. Alteration and mineralization

The following description of alteration in the Kidd Creek mine is

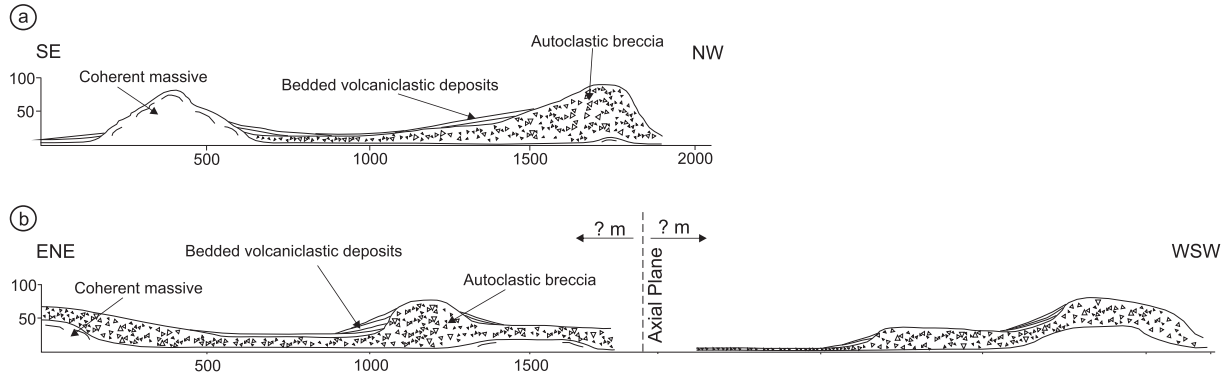

Fig. 18. Cross-sections showing the distribution of aphyric rhyolite. (a) E-W cross-section through the northern limb of the NR anticline. (b) NE-SW cross-section across both limbs of the NR anticline. See Fig. 16a for the location of sections. Vertical exaggeration = x2.

from Koopman et al. (1999). Footwall alteration to the Kidd Creek orebody consists of a broad semiconformable zone of sericite alteration and a more localized area of chlorite alteration, all within a broader zone of silicification. Pervasive silicification is the earliest stage of alteration at Kidd Creek and is characterised by varying degrees of replacement of the rock by microcrystalline quartz resulting in elevated SiO_2 (> 79%) values. The most intensely silicified rocks occur immediately below the massive sulfides of the Kidd Creek deposit and up to 150 to 200 m below the ore horizon. Silica alteration was followed by pervasive and patchy sericite alteration that occurs as fine-grained disseminated sericite, with minor chlorite in a weakly to moderately silicified rhyolite. Intense sericite alteration consists of greater than 3 wt% K_2O and less than 2 wt% Na_2O. Sericite alteration forms a halo around the Kidd Creek deposit and grades into a chlorite-sericite alteration near the chalcopyrite stringer zone. Minor chlorite alteration in the Kidd Creek rhyolites occur throughout as fine, disseminated grains, intergrown with microcrystalline quartz and sericite. Moderate to intense chlorite alteration occurs as discordant zones below the massive sulfide lenses but typically does not extend more than 50 m into the footwall. Massive chlorite is locally well developed within conformable zones of chalcopyrite mineralization and has MgO values greater than 2 wt%, and Fe_2O_3 and FeO values greater than 6 and 4 wt%, respectively. The chlorite is typically coarse-grained and replaces rhyolitic tuff units forming discrete, strata bound lenses of black, chlorite-rich rock.

In this paper VMS-related alteration within the NR is defined, and its distribution assessed, using: (1) spatial variation in Na_2O and K_2O to show the distribution of sericite alteration, because they indicate feldspar destruction and the development of sericite that is typical of sericite alteration zones; (2) the distribution of $Fe_2O_{3(T)}$ and MgO, because they reflect chlorite alteration; and (3) SiO_2, which shows the amount of silicification. Areas of mineralization are shown using Cu and Zn values.

Major element data for both the QP and aphyric rhyolites are the same with few exceptions, namely for subtle variations in Al_2O_3 and TiO_2, therefore the least altered QP rhyolite composition used by Prior et al. (1999a) is used as a reference to assess alteration in aphyric rhyolites. Alteration is shown using the average values for Na_2O, K_2O, chlorite index, and SiO_2 calculated from all samples through the entire thickness of aphyric and QP rhyolite intersected in each drill hole; the number of samples per drill hole ranges from 5 to 20, depending on the length of the intersection, with samples collected roughly 10 m apart.

9.1. Silica alteration

Moderate pervasive silicification occurs throughout the coherent portions of the domes and flows, but the most intensely silicified areas (≥78 wt% SiO_2) occur within rhyolite domes or flows. The most intensely silicified zones also correspond with areas of sericite alteration and base metal mineralization. As with K_2O and Na_2O (sericite), and FeO and MgO (chlorite) alteration, silicification decreases with increasing distance from the rhyolite domes. Because moderate silicification is pervasive throughout the rhyolite domes and flows silica alteration is not depicted graphically in this paper.

9.2. Sericite alteration

The least altered sample of QP rhyolite from the Kidd Creek mine contains 1.98 wt% K_2O (Prior et al., 1999a). Any sample with a K_2O value greater than 2.0 wt% was contoured as illustrated in Figs. 16 and 17b. The highest K_2O values (4 wt%) occur within aphyric rhyolite domes where they define relatively small areas of intensely altered rhyolite surrounded by progressively decreasing amounts of K_2O

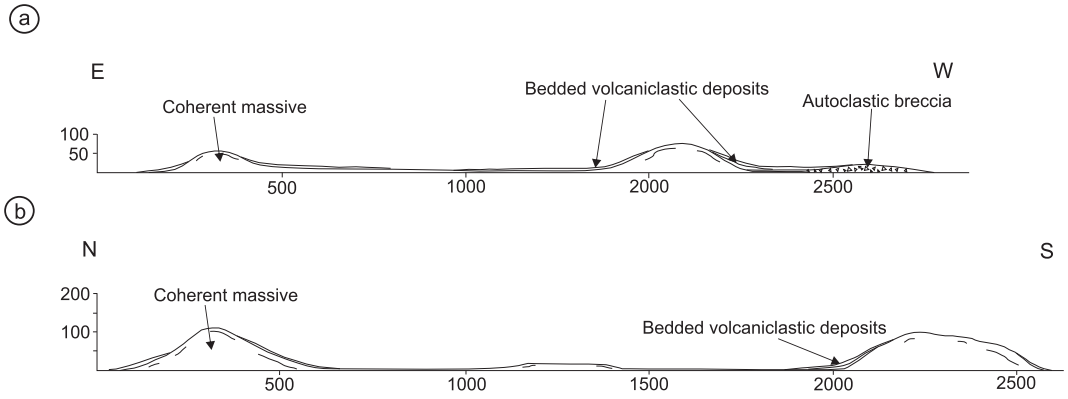

Fig. 19. Cross-sections showing the distribution of QP rhyolite. (a) NNE-SSW cross-section through the QP rhyolite domes of the northern limb of the NR anticline. (b) N-S cross-section through the QP rhyolite domes of the southern limb of the NR anticline. See Fig. 17a for the location of sections. No vertical exaggeration.

(Fig. 16b). The intensity of sericite alteration within aphyric rhyolite intersected in each drill hole appears to be relatively uniform as individual samples within each intersection vary by less than 0.5 wt%. Areas containing the highest K_2O values (> 3.5 wt%) also correspond with areas of mineralization indicated by elevated Cu and Zn values (Fig. 16a).

Potassium enrichment (up to 4 wt% K_2O) does occur in the hanging-wall QP rhyolite, though it is much less extensive than the K_2O alteration in the underlying aphyric rhyolite. In the QP rhyolite the highest K_2O values do not correspond with the rhyolite domes, nor do they correspond with the highest values for K_2O in the underlying aphyric rhyolite (Fig. 17b).

The least altered sample of QP rhyolite from the Kidd Creek mine has a value of 2.56 wt% Na_2O (Prior et al., 1999a). Any sample with less than 2.5 wt% Na_2O was contoured as illustrated in Figs. 16 and 17c. The lowest Na_2O values occur in aphyric rhyolite domes where they define a relatively small area of intensely altered rhyolite surrounded by increasing amounts of Na_2O (Fig. 16c). Within individual aphyric rhyolite intersections Na_2O values vary by less than 0.5 wt%.

Depletion in Na_2O occurs in the QP rhyolite, though it is much less intense and restricted in its occurrence, as compared with that in the underlying aphyric rhyolite. Thus, the most intensely Na_2O depleted and K_2O enriched areas in QP rhyolite do not directly overlie the most intensely Na_2O depleted and K_2O enriched areas in the aphyric rhyolite (Fig. 17c).

9.3. Chlorite alteration

The least altered sample of QP rhyolite from the Kidd Creek mine has a chlorite index ($Fe_2O_3 + MgO/Fe_2O_3 + MgO + 2CaO + 2Na_2O$) of 0.14 (Prior et al., 1999a). Any sample with a chlorite index value greater than 0.14 is contoured in Fig. 16d. Chlorite alteration in the aphyric rhyolite very closely mirrors Na_2O, K_2O and SiO_2 alteration in the rhyolite. Chlorite index values are highest (> 0.60) in the centers of rhyolite domes or flows, tend to decrease away from the rhyolite domes or flows, and are locally intense in areas of autobreccia adjacent to the rhyolite domes (Fig. 16d). Within individual intersections of rhyolite chlorite index values vary by less than 0.10.

9.4. Mineralization

Copper values ranging from 0.30 to 2.75%, and Zn values from 0.60 to 6.01% occur on both the northeast and southwest limbs of the NR anticline. Areas with Zn values greater than 0.60%, and Cu values greater than 0.30% are shown in Fig. 16a. Areas of Cu and Zn mineralization, for the most part, correspond with rhyolite domes and with areas of strong sericite and chlorite alteration. The one exception occurs along the northeast limb where mineralization (Zn = 0.70–1.14%; Cu = 0.31–0.60%) occurs within flank breccias of a large unexplored aphyric rhyolite dome at the edge of the study area. On the southwest limb of the NR fold significant Cu and Zn values occur on the flank of the Kidd Creek orebody.

9.5. Interpretation of alteration and mineralization

Trends defined by the distribution of silicification, sericite, and chlorite alteration, as well as the Zn and Cu mineralization within aphyric rhyolite follow the same general trends of the aphyric rhyolite ridges and domes. Alteration and mineralization are most intense within the rhyolite ridges and domes, indicating that the volcanic structures through which the rhyolite was extruded also served as the conduits for hydrothermal fluids. There is also significant alteration in the breccias on the flanks of the domes or flows, perhaps because of their permeability and proximity to volcanic structures that controlled the location of ridges and domes and acted as conduits for hydrothermal fluids. Within individual drill holes values do not vary by more than 0.5 wt%, for K_2O and Na_2O, or 0.10 for the chlorite index. Thus, the entire rhyolite interval was uniformly altered indicating that the hydrothermal system, where developed, was pervasive.

As in the Kidd Creek mine stratigraphy (Prior et al., 1999a; Hannington et al., 1999b), sericite and silica alteration does occur in the hanging-wall QP rhyolite although it is weak, indicating that the hydrothermal system responsible for the alteration in the NR was still active during eruption of the QP rhyolite. The non-correspondence between areas of alteration in the aphyric and overlying QP rhyolites indicates that the different synvolcanic structures inferred to have controlled the extrusion of aphyric and QP rhyolite, also controlled hydrothermal fluids leading to alteration of the rhyolites.

Significant mineralization (Cu > 0.5 wt% and Zn > 1.0 wt%) occurs within aphyric rhyolite on the southern limb of the fold near the Kidd Creek orebodies where it likely represents the weakly mineralized edge of the massive Kidd Creek deposit. There is also significant Cu and Zn mineralization on the northeast limb of the NR fold in an aphyric rhyolite dome that appears to continue beyond the study area. It is also important to note that the extent of the aphyric and QP rhyolites shown in Figs. 13 and 14a is only part of a larger rhyolite dome field that may contain significant mineralization.

10. Discussion

Detailed volcanic lithofacies definition and distribution, including the recognition of rhyolite flow-dome complexes that define synvolcanic faults, and the identification of hydrothermal alteration are essential in locating VMS deposits. VMS deposit formation is largely controlled by synvolcanic faults; therefore, the identification such features is critical in exploring for VMS deposits. Synvolcanic faults represent highly focused fluid pathways that also facilitate the accumulation of volcaniclastic debris, due to movement along these faults during subsidence, and rhyolite flow-dome complexes provide abundant permeable volcaniclastic deposits, all controlling factors in the formation of VMS deposits.

10.1. Linking the NR and Kidd Creek volcanic settings

A 3D volcanic reconstruction of the NR has allowed an examination of the larger Kidd Creek volcanic and ore-forming environment. Previous workers (Bleeker, 1999; Hannington et al., 1999b) proposed that subsidence occurred along a synvolcanic extensional fault on the northern margin of the North and Central orebodies and that this fault was critical in focusing hydrothermal upflow in the formation of the orebodies. Fig. 20 is a schematic block diagram, post-aphyric rhyolite emplacement, that shows the spatial association of the aphyric rhyolite isopach map from Fig. 16a in the context of Bleeker's (1999) reconstruction of the primary depositional setting of the Kidd Creek orebodies. While the synvolcanic fault depicted in this diagram was certainly critical in the formation of the orebodies and the host rhyolitic units, this study shows that is did not entirely restrict the Kidd Mine stratigraphy and zone of hydrothermal alteration as it clearly continues some 2 km to the north and some 2–3 km to the northeast to the area of the NR. We know from this study that the aphyric rhyolite, and QP rhyolite flow-domes (with the same orientation as those in the Kidd mine area) as well as basalt flows (including the lowermost low TiO_2 flows) continue beyond the northern limit of the North and Central orebodies and the fault they define. Thus, the volcanic and hydrothermal setting in which Kidd Creek orebodies formed, including the associated synvolcanic structures through which the rhyolite domes were emplaced, and which focused fluid upflow, includes the NR and extends at least 2 km to the north and at least 2 km to the northeast of the Kidd Creek deposit (Fig. 20).

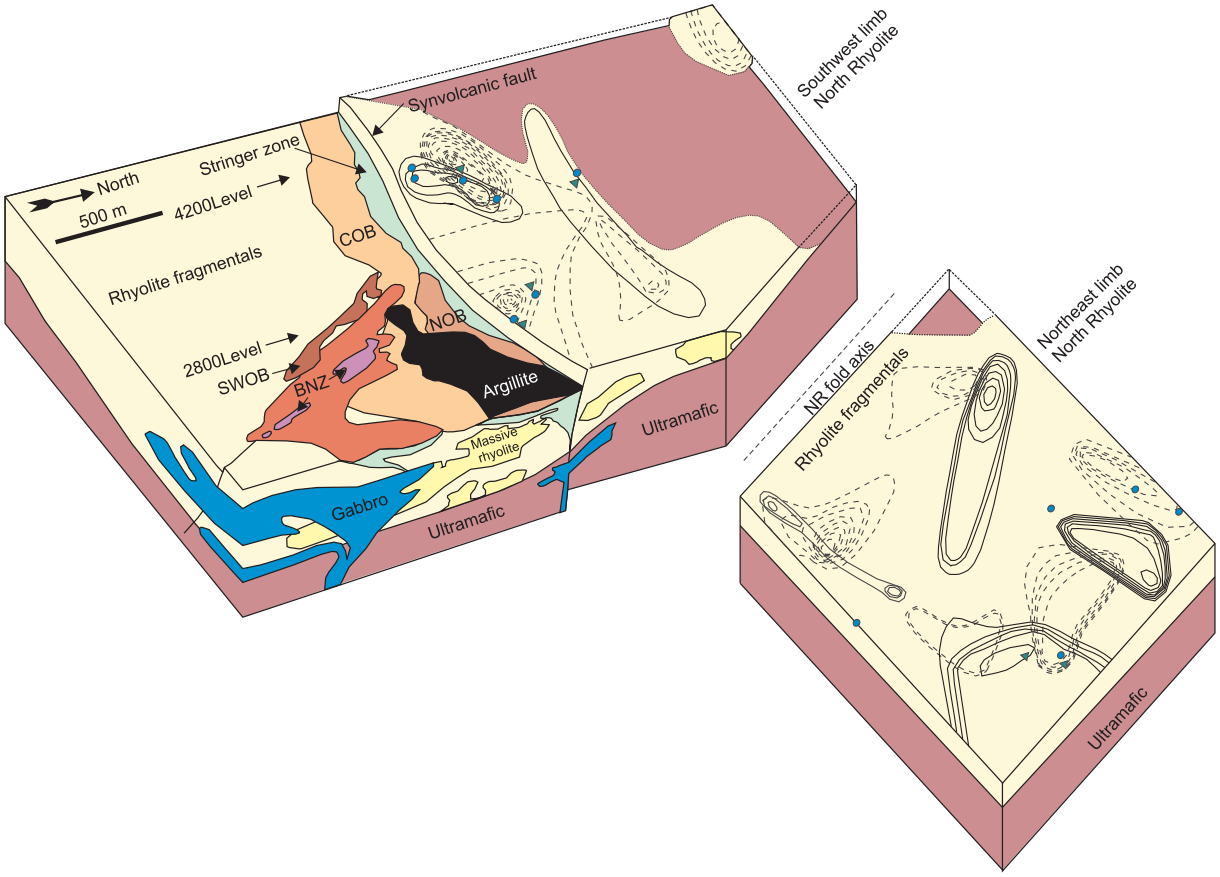

Fig. 20. Schematic block diagram showing the deposition environment of the Kidd Creek deposit (modified from Bleeker, 1999) with the addition of the volcanic reconstruction of the aphyric rhyolite of the NR as an overlay (rhyolite isopachs and mineralization as in Fig. 13a) on blocks representing the southwest and northeast limbs of the NR fold. SOB, COB and NOB = South, Central and North Orebodies of the Kidd Creek Deposit.

10.2. Controls on rhyolite morphology and distribution

Given the preponderance of ancient and modern VMS deposits to be associated with rhyolitic rocks (e.g. Noranda, Sturgeon Lake, Flin Flon, Snow Lake, Kuroko, Myojin Knoll Sunrise deposit), the recognition of the size, shape and distribution of rhyolite flow-domes is an important consideration in locating VMS deposits. In the NR, rhyolite flow-domes have the same orientation as those in the Kidd Creek mine area, where they are elongate parallel to the orebodies (Prior, 1996), evidence of a strong structural control on the emplacement of both the rhyolite flow-domes as well as alteration and mineralization. The rhyolite flow-domes of the NR are elongate, ridge-like structures, up to 115 m high and 2 km long, that represent long-lived synvolcanic faults that were reactivated as magma and hydrothermal fluid pathways and controlled the eruption and distribution of rhyolite. The narrow, ridge-like shape of the rhyolite flow-dome complexes suggest they were fissure-fed.

The faults controlling rhyolite eruption would have also aided in concentrating porous volcaniclastic deposits on and around the rhyolite ridges, creating a favorable environment for hydrothermal fluid circulation and sulfide precipitation. At Noranda rhyolite bodies also tend to form elongate flow-dome complexes and as such a similar interpretation has been made for long-lived synvolcanic faults that controlled rhyolite distribution, hydrothermal fluids discharge and mineralization at Noranda (Gibson et al., 1999; Galley et al., 2007). Within the Myojin Knoll caldera a 250 m-thick rhyolite dome occurs along the southeastern caldera wall, suggesting its distribution was also controlled by a synvolcanic fault (Fiske et al., 2001).

The minimum estimated volume of the aphyric and QP rhyolite flow-domes of the NR is $\sim 0.2\,km^3$ and when added to the estimated total volume of aphyric and QP rhyolite within the Kidd Mine area the total rhyolite volume is $\sim 0.5\,km^3$. Compared with the $\sim 0.6\,km^3$ volume of the Myojin Knoll dome (Fiske et al., 2001) the rhyolite flow-domes of the Kidd Creek caldera are individually smaller, but overall have a similar total volume to the rhyolite dome of the Myojin Knoll caldera. They also have similar volume to the ~ 0.2–$0.4\,km^3$ rhyolite associated with the Hébécourt Formation of the Blake River Group (Rogers et al., 2014). However, the 900 m thick rhyolite sequence of the Horne deposit in Noranda (Gibson et al., 2000) would have a considerably larger volume, on the order of $1\,km^3$. As a minimum estimate the volume of rhyolite at Kidd Creek is comparable to both Archean and modern rhyolite-hosted VMS examples.

10.3. Distribution of hydrothermal alteration

In addition to recognizing synvolcanic faults and volcanic lithofacies distribution, the recognition of hydrothermal alteration is imperative in locating VMS deposits. Semi-conformable distribution of silica, sericite and chlorite alteration is characteristic of both Archean (e.g. Noranda; Gibson et al., 1983) and modern (e.g. PACMANUS; Lackschewitz et al., 2004) VMS systems. Chlorite is recognized as representing a vent proximal alteration zone and is commonly associated with copper-stringer type mineralization in VMS deposits, whereas sericite alteration occurs more distal to the vent (Galley et al., 1993).

In terms of mineralogy and structural controls, the hydrothermal characteristics of the Kidd Creek system are typical of both ancient and modern VMS deposits (e.g., Gibson et al., 1999; Hudak et al., 2003; Large et al., 2001, Fiske et al., 2001, Mueller et al., 2009). Silica, sericite and chlorite alteration occur in the aphyric rhyolite of the Kidd Creek mine stratigraphy and throughout the NR thereby extending the Kidd Creek hydrothermal alteration zone to include the NR. Alteration

is most intense proximal to rhyolite domes of the NR indicating the same volcanic structures responsible for the extrusion of the rhyolite also focused ascending hydrothermal fluids responsible for alteration and the formation of the orebodies. It is an interesting observation that hydrothermal alteration within the NR is highly focused on the southwest limb with more broad zones of alteration on the northwest limb. Although hydrothermal fluid upflow on the northwest limb was still focused along the same structures that controlled rhyolite distribution (as on the southeast limb), perhaps it is the intersection of two different orientations of structures controlling rhyolite ridge formation and hydrothermal fluid upflow on the northwest limb that has resulted on more broad distribution of hydrothermal alteration.

The QP rhyolite of the NR shows minor sericite and chlorite alteration, evidence that the hydrothermal system was still active during the extrusion of the QP rhyolite, even kilometers from the Kidd Creek deposit. Therefore, the Kidd Creek deposit is part of a much larger hydrothermal system whose total extent remains unknown, but whose estimated size has greater than doubled from our previous understanding.

11. Conclusions

Detailed mapping (underground and through core logging) of complex lithofacies and lithofacies distribution, in combination with lithogeochemical data analysis, has resulted in a 3D reconstruction of the larger volcanic and ore-forming environment at Kidd Creek. The model presented has resulted in a doubling of the estimated size of the rhyolite field at Kidd Creek and clearly links rhyolitic volcanism of the NR with synvolcanic structures that acted as magma pathways and also focused zones of hydrothermal upflow leading to anomalous copper and zinc values.

Our study shows that the NR is the folded continuation of the Kidd Creek mine stratigraphy, and from oldest to youngest comprises komatiites, aphyric rhyolite and associated volcaniclastic rocks, QP rhyolite and associated volcaniclastic rocks, and basalt flows. All lithologies mapped within the NR are identical in terms of lithofacies and lithogeochemistry to those of the Kidd Creek mine stratigraphy. Recognition of the continuation of the Kidd Creek mine stratigraphy to the NR and the lack of any significant changes in either the rhyolite or basalt thicknesses, or facies, between the Kidd Creek mine area and the NR suggests that the graben wall, interpreted to be just north of the North and Central orebodies (Bleeker 1999) did not restrict the Kidd Creek mine stratigraphy from continuing north to the area of the NR.

The orientation of rhyolite domes, both in the NR and in the Kidd Creek mine area, are the same and correspond to the orientation of the Kidd Creek orebodies. The aphyric rhyolite of the NR contains significant sericite and chlorite alteration, and anomalous copper and zinc. The alteration and mineralization are most intense over the thickest portions of rhyolite domes and ridges, indicating a strongly pronounced structural control on the distribution of rhyolite and that structures that acted as magmas pathways were reactivated as hydrothermal fluid pathways and consequently controlled mineralization. The presence of alteration along with copper and zinc mineralization in the NR, is further evidence that the structure (graben wall) that largely focused hydrothermal upflow in forming the North and Central orebodies does not mark the limit of the hydrothermal alteration, although it is true that alteration beyond this structure (i.e., with the NR stratigraphy) is much less than in the Kidd Mine stratigraphy and certainly, thus far, no significant amount of mineralization has been found within the NR. Still, the rhyolite field and hydrothermal alteration zone of Kidd Creek is much larger than was previously thought, thereby expanding the zone of potential mineralization.

This study shows that detailed multidimensional modelling of geological complexities, accomplished through spatial data analysis of underground and drill core data, when coupled with detailed lithogeochemistry, and the 'unfolding' of multiple deformations through 3D modelling software, can result in a 3D reconstruction of ancient, polydeformed volcanic and ore-forming environments. The 3D model demonstrates the lithological and primary structural control on VMS ore-formation. Our volcanic reconstruction shows not only the control that primary volcanic features have on focusing hydrothermal fluid upflow, and therefore ore-formation, but also how these volcanic structures can be translated into mappable spatial proxies that can be used in exploration targeting.

Acknowledgements

This study was funded by Falconbridge Ltd. and a Natural Sciences and Engineering Research Council (NSERC) of Canada Discovery Grant held by H.G. Gibson. M. DeWolfe would like to acknowledge assistance at the mine site by the staff in the geology department including, but not limited to, R. Lafond, M. Lafond, S. Gibbins, P. Simunovic, M. Schonfield, P. Calloway, and M. Collison. The authors would like to thank C. Partin and J. Pollock for review a draft of this manuscript. Special thanks are given to Profs. M. Hannington and P.-S. Ross whose thoughtful reviews benefited the manuscript greatly.

Appendix A. Supplementary data

The appendices contain underground maps (Appendix A), petrographic analyses (Appendix B), geochemical analyses (Appendix C) and details of how the NR was 'unfolded' in the reconstruction (Appendix D).

Supplementary data associated with this article can be found, in the online version, at https://doi.org/10.1016/j.oregeorev.2018.07.008.

References

Ayer, J., Amelin, Y., Corfu, F., Kamo, S., Ketchum, J., Kwork, K., Trowell, N., 2002. Evolution of the southern Abitibi greenstone belt based on U-Pb geochronology: autochthonous volcanic construction followed by plutonism, regional deformation and sedimentation. Precambr. Res. 115, 63–95.

Ayer, J.A., Thurston, P.C., Bateman, R., Dubé, B., Gibson, H.L., Hamilton, M.A., Hathway, B., Hocker, S.M., Houlé, M.G., Hudac, G., Ispolatov, V.O., Lafrance, B., Lesher, C.M., MacDonald, P.J., Péloquin, A.S., Piercey, S.J., Reed, L.E., Thompson, P.H. 2005. Overview of results of the Greenstone Architecture Project: Discover Abitibi Initiative. Ontario Geological Survey Open File Report 6154, 146p.

Barrie, T.C., 1995. Zircon thermometry of high-temperature rhyolites near volcanic associated massive sulfide deposits, Abitibi Subprovince, Canada. Geology 23, 169–172.

Barrie, T.C., 1999. Komatiite flows of the Kidd Creek footwall Abitibi subprovince, Canada. Econ. Geol. Monograph 10, 143–162.

Barrie, C.T., Davis, D.W., 1990. Timing of magmatism and deformation in the Kamiskotia-Kidd creek area, western Abitibi subprovince, Canada. Precambr. Res. 46, 217–240.

Barrie, T.C., Cousens, B.L., Hannington, M., Bleeker, W., Gibson, H., 1999. Lead and Neodymium isotope systematics of the Kidd Creek Mine stratigraphic sequence and ore, Abitibi Subprovince, Canada. Econ. Geol. Monograph 10, 511–524.

Bateman, R., Ayer, J.A., Dubé, B., 2008. The Timmins-Porcupine gold camp, Ontario: anatomy of an Archean greenstone belt and ontogeny of gold mineralizations. Econ. Geol. 103, 1285–1308.

Beresford, S.W., Cas, R.A.F., 2001, Komatiitic invasive lava flows, Kambalda, western Australia. In: Barnes, S.-J., Crocket, J.H., Martin, R.F. (Eds.), Ore-forming Processes in Dynamic Magmatic Systems. Canadian Mineralogist, vol. 39, part 2, pp. 525–535.

Berger, B., Ayer, J., McNicoll, V.J., Bleeker, W., 2007. The Kidd-Munro project: stratigraphy of the Kidd-Munro assemblage in Prosser Tp. and area based on geology, geochemistry and new geochronology. Ontario Geological Survey Open File Report 6213 5-1–5-8.

Berger, B.R., Bleeker, W., van Breemen, O., Chapman, J.B., Peter, J.M., Layton-Matthews, D., Gemmell, J.B. 2011. Results from the Targeted Geoscience Initiative III Kidd–Munro Project. Ontario Geological Survey Open File Report 6258, 142p.

Bleeker, W., 1994. The Giant Kidd Creek Massive Sulfide Deposit: A New Perspective. Falconbridge Ltd., Timmins, Ontario, pp. 88 Unpublished company report.

Bleeker, W., 1995, Surface Geology of the Porcupine Camp. Canada Geological Survey Open-File Report 3141, pp. 13–37.

Bleeker, W., 1999. Structure, stratigraphy, and primary setting of the Kidd Creek volcanogenic massive sulfide deposit: a semiquantitative reconstruction. Econ. Geol. Monograph 10, 71–121.

Bleeker, W., Parrish, R.R., 1996. Stratigraphy and U-Pb zircon geochronology of Kidd Creek: implications for the formation of giant volcanogenic massive sulphide deposits and the tectonic history of the Abitibi greenstone belt. Can. J. Earth Sci. 33, 1213–1231.

Bleeker, W., Hester, B.W., 1999. Discovery of the Kidd Creek massive sulfide orebody: a

historical perspective. Econ. Geol. Monograph 10, 31–42.
Bleeker, W., van Breeman, O., 2011, New geochronological, stratigraphic and structural observations on the Kidd-Munro assemblage and the terrane architecture of the south-central Abitibi greenstone belt, Superior craton, Canada. In: Result from the Targeted Geoscience Initiative III Kidd-Munro Project, Ontario Geological Survey, open File Report 6258, 142.
Bleeker, W., Parrish, R.R., Sager-Kinsman, A., 1999. High-precision U-Pb geochronology of the late Archean Kidd Creek deposit and Kidd Volcanic Complex. Econ. Geol. Monograph 10, 43–70.
Card, K.D., 1990. A review of the superior province of the Canadian Shield, a product of Archean accretion. Precambr. Res. 48, 99–156.
Comba, C.D.A., Binney, W.P., Stewart, R.D., Cunnison, K.M., Mullen, D.V., 1986, Timmins, Ontario: exceptional exposures of Archean subaerial and shallow subaqueous volcanic rocks and associated ore deposits. Geological Association of Canada Field Trip Guidebook 5, pp. 25.
Corfu, F., Krough, T.E., Kwok, Y.Y., Jensen, L.S., 1989. U-Pb geochronology in the southwestern Abitibi greenstone belt, Superior province. Can. J. Earth Sci. 26, 1747–1763.
Corfu, F., 1993. The evolution of the southern Abitibi greenstone belt in light of precise U-Pb geochronology. Econ. Geol. 88, 1323–1340.
Debreil, J.-A., Ross, P.-S., Mercier-Langevin, P., 2018. The Matagami district, Abitibi Greenstone Belt, Canada: volcanic controls on Archean volcanogenic massive sulfide deposits associated with voluminous felsic volcanism. Econ. Geol. 113, 891–910.
Dinel, E., Bleeker, W., Ayer, J., Dubé, B., 2008. Structurla investigation and mineral potential of the Kidd-Munro assemblage in Clergue and Walker townships. Geol. Survey Canada, Curr. Res. 2008-23 10.
Dubé, B., Mercier-Langevin, P., Hannington, M., Lafrance, B., Gosselin, G., Gosselin, P., 2007. The LaRonde Penna world-class Au-rich volcanogenic massive sulfide deposit, Abitibi, Québec: mineralogy and geochemistry of alteration and implications for genesis and exploration. Econ. Geol. 102, 633–666.
Fisher, R.V., 1961. Proposed classification of volcaniclastic sediments and rocks. Geol. Soc. Am. Bull. 72, 1395–1408.
Fiske, R.S., Naka, J., Iizasa, K., Yuasa, M., Klaus, A., 2001. Submarine silicic caldera at the front of the Izu-Bonin Arc, Japan: voluminous seafloor eruptions of rhyolite pumice. Geol. Soc. Am. Bull. 113, 813–824.
Franklin, J.M., Thorpe, R.I., 1982. Comparative metallogeny of the Superior, Slave, and Churchill provinces. Geol. Assoc. Can. Spec. Pap. 25, 3–90.
Fyon, J.A., Breaks, F.W., Heather, K.B., Jackson, S.L., Muir, T.L., Stott, G.M., Thurston, P.C., 1991. Metallogeny of metallic mineral deposits of the Superior Province of Ontario. Ontario Geol. Survey Special Vol. 4 (2), 1090–1174.
Galley, A.G., 1993. Characteristics of semi-conformable alteration zones associated with volcanogenic massive sulphide districts. J. Geochem. Explor. 48, 175–200.
Galley, A., Hannington, M., Jonasson, I., 2007. Volcanogenic massive sulphide deposits. 5. Geological Association of Canada Mineral Deposits Division Special Publication, pp. 141–161.
Gibson, H.L., 1990. The Mine Sequence of the Central Noranda Volcanic Complex: Geology, Alteration, Massive Sulfide Deposits and Volcanological Reconstruction (Unpublished Ph.D. thesis). Carleton University, Ottawa, Ontario, pp. 800.
Gibson, H.L., Morton, R.L., Hudak, G.J., 1999, Submarine volcanic processes, deposits, and environments favourable for the location of volcanic associated massive sulfide deposits. In: Barrie, C.T., Hannington, M.D. (Eds.), Volcanic Associated Massive Sulfide Deposits: Processes and Examples in Modern and Ancient Settings. Reviews in Economic Geology, vol. 8, pp. 13–49.
Gibson, H.L., Kerr, D.J., Cattalani, S., 2000. The Horne Mine: geology, history, influence on genetic models, and a comparison to the Kidd Creek Mine. Explor. Mining Geol. 9, 91–111.
Gibson, H., Galley, A., 2007. Volcanogenic massive sulphide deposits of the Archean Noranda district, Quebec. In: Goodfellow, W.D. (Ed.), Mineral Deposits of Canada: A Synthesis Of Major Deposits Types, District Metallogeny, the Evolution of Geological Provinces, and Exploration Methods. Geological Association of Canada, Mineral Deposits Division, pp. 533–552.
Giordano, D., Russell, J.K., Dingwell, D.B., 2008. Viscosity of magmatic liquids: a model. Earth Planet Sci. Lett. 271, 123–134.
Hannington, M.D., Barrie, C.T., Bleeker, W., 1999a. The Giant Kidd Creek volcanogenic massive sulfide deposit, Western Abitibi Subprovince, Canada: preface and introduction. Econ. Geol. Monograph 10, 1–28.
Hannington, M.D., Bleeker, W., Kjarsgaard, I., 1999b. Sulfide Mineralogy, Geochemistry, and Ore Genesis of the Kidd Creek Deposit: Part I. North, Central, and South Orebodies. Econ. Geol. Monograph 10, 163–224.
Heather, K.B., Percival, J.A., Moser, D., Bleeker, W. (Eds.), 1995, Tectonics and Metallogeny of Archean Crust in the Abitibi-Kapuskasing-Wawa Region. Canada Geological Survey Open-File Report 3141, pp. 148.
Hudak, G.J., Morton, R.L., Franklin, J.M., Peterson, D.M., 2003. Morphology, distribution, and estimated eruption volumes for intracaldera tuffs associated with volcanic-hosted massive sulfide deposits in the Archean Sturgeon Lake Caldera Complex, northwestern Ontario. In: In: White, J.D., Smellie, J.L., Clague, D.A. (Eds.), Explosive subaqueous volcanism 140. American Geophysical Union, Geophysical Monograph Series, pp. 345–359.
Huston, D.L., Taylor, B.E., Bleeker, W., Stewart, B., Cook, R., Koopman, E., 1995. Isotope mapping around the Kidd Creek deposit, Ontario: Application to exploration and comparison with other geochemical indicators. Explor. Min. Geol. 4, 175–187.
Ispolatov, V., Lafrance, B., Dubé, B., Creaser, R., Hamilton, M., 2008. Geologic and structural setting of gold mineralization in the Kirkland LakeLarder Lake gold belt, Ontario. Econ. Geol. 103, 1309–1340.
Jackson, S.L., Sutcliffe, R.H., 1990. Central Superior province geology: evidence for an allochthonous ensimatic southern Abitibi greenstone belt. Can. J. Earth Sci. 27, 582–589.
Jackson, S.L., Fyon, J.A., 1991. The western Abitibi subprovince in Ontario. Ontario Geol. Survey Special Vol. 4 (1), 405–482.
Jackson, S.L., Cruden, A.R., 1995. Formation of the Abitibi greenstone belt by arc-trench migration. Geology 23, 471–474.
Koopman, E.R., Hannington, M.D., Santiguida, F., Cameron, B.I., 1999. Petrology and geochemistry of proximal hydrothermal alteration in the Mine Rhyolite at Kidd Creek. Econ. Geol. Monograph 10, 267–296.
Kretz, R., 1983. Symbols for rock-forming minerals. AM. Mineral. 68, 277–279.
Lackschewitz, K.S., Devey, C.W., Stoffers, P., Botz, R., Eisenhauer, A., Kummetz, M., Schmidt, M., Singer, A., 2004. Mineralogical, geochemical and isotopic characteristics of hydrothermal alteration processes in the active, submarine, felsic-hosted PACMANUS field, Manus Basin, Papua New Guinea. Geochimica et Cosmochimica Acta 68, 4405–4427.
Langford, F.F., Morin, J.A., 1976. The development of the Superior Province of northwestern Ontario by merging island arcs. Am. J. Sci. 276, 1023–1034.
McNicoll, V., Goutier, J., Dubé, B., Mercier-Langevin, P., Ross, P.-S., Dion, C., Monecke, T., Legault, M., Percival, J., Gibson, H., 2014. U-Pb geochronology of the blake river group, abitibi greenstone belt, Quebec, and implications for base metal exploration. Econ. Geol. 109, 27–59.
Mercier-Langevin, P., Dubé, B., Lafrance, B., Hannington, M., Galley, A., Moorhead, J., Gosselin, P., 2007. Metallogeny of the Doyon-Bousquet-LaRonde mining camp, Abitibi Greenstone Belt, Quebec. In: Goodfellow, W.D. (Ed.), Mineral Deposits of Canada: A Synthesis of Major Deposits Types, District Metallogeny, the Evolution of Geological Provinces, and Exploration Methods. Geological Association of Canada, Mineral Deposits Division, pp. 673–701.
Mercier-Langevin, P., Goutier, J., Ross, P.-S., McNicoll, V., Monecke, T., Dion, C., Dubé, B., Thurston, P., Bécu, V., Gibson, H., Hannington, M., Galley, A., 2011. The Blake River Group of the Abitibi Greenstone Belt and its unique VMS and gold-rich VMS endowment. Geological Survey of Canada, Open File, 6869, 1–61.
Mercier-Langevin, P., Gibson, H.L., Hannington, M.D., Goutier, J., Monecke, T., Dubé, B., Houlé, M., 2014. A special issue on archean magmatism, volcanism, and ore deposits: Part 2. volcanogenic massive sulfide deposits preface. Econ. Geol. 109 (1), 1–9.
Large, R.R., Gemmell, J.B., Paulick, H., Huston, D.L., 2001. The alteration box plot: a simple approach to understanding the relationship between alteration mineralogy and lithogeochemistry associated with volcanic-hosted massive sulfide deposits. Econ. Geol. 96, 957–971.
Lesher, C.M., Goodwin, A.M., Campbell, I.H., Gorton, M.P., 1986. Trace-element geochemistry of ore-associated and barren, felsic metavolcanic rocks in the Superior Province, Canada. Can. J. Earth Sci. 23, 222–237.
Ludden, J.N., Hubert, C., 1986. Geological evolution of the Late Archean Abitibi greenstone belt of Canada. Geol. Mag. 123, 123–166.
Ludden, J.N., Hubert, C., Gariepy, C., 1986. The tectonic evolution of the Abitibi greenstone belt of Canada. Geology 14, 707–711.
Manley, C.R., Fink, J.H., 1987. Internal textures of rhyolite flows as reveled by research drilling. Geology 15, 549–552.
McPhie, J., Doyle, M., Allen, R., 1993. Volcanic Textures: A Guide to the Interpretation of Textures in Volcanic Rocks. University of Tasmania, Center for Ore Deposits and Exploration Studies, Hobart, pp. 196.
Monecke, T., Gibson, H., Dubé, B., Laurin, J., Hannington, M.D., Martin, L., 2008. Geology and volcanic setting of the Horne deposit, Rouyn Noranda, Quebec: Initial results of a new research project. Geol. Survey Canada Curr. Res. 2008-9 16.
Monecke, T., Gibson, H., Goutier, J., 2017. Volcanogenic massive sulfide deposits of the Noranda camp. Rev. Econ. Geol. 19, 169–223.
Mortensen, J.K., 1993. U-Pb geochronology of the eastern Abitibi subprovince. Part 2. Noranda-Kirkland Lake area. Can. J. Earth Sci. 30, 29–41.
Mueller, W.U., Stix, J., Corcoran, P.L., Daigneault, R., 2009. Subaqueous calderas in the Archean Abitibi greenstone belt: An overview and new ideas. Ore Geol. Rev. 35, 4–46.
Nunes, P.D., Pyke, D.R., 1980. Geochronology of the Abitibi metavolcanic belt, Timmins-Matchewan area – progress report. Ontario Geol. Misc. Papers 92, 34–39.
Nunes, P.D., Pyke, D.R., 1981. Time stratigraphic correlation of the Kidd Creek orebody with volcanic rocks south of Timmins, Ontario, as inferred from zircon U-Pb ages. Econ. Geol. 76, 944–951.
Percival, J.A., Card, K.D., 1985. Structure and the evolution of the Archean crust in central Superior province, Canada. Geol. Assoc. Can. Spec. Pap. 28, 179–192.
Prior, G.J., 1996. Volcanology and Geochemistry of Archean Rhyolites and Related Volcaniclastic Rocks Associated with the Kidd Creek Volcanogenic Massive Sulfide Deposit, Abitibi Greenstone Belt, Superior Province, Canada (Unpublised Ph.D. thesis). Carleton University, Ottawa, Canada, pp. 302.
Prior, G.J., Gibson, H.L., Watkinson, D.H., Cook, R., 1999a. Anatomy, lithogeochemistry and emplacement mechanisms for the QP rhyolite, Kidd Creek Mine, Timmins, Ontario. Econ. Geol. Monograph 10, 123–142.
Prior, G.J., Gibson, H.L., Watkinson, D.H., Cook, R., Hannington, M., 1999b. Rare earth and high field strength element geochemistry of the Kidd Creek rhyolites, Abitibi greenstone belt, Canada: Evidence for Archean felsic volcanism and massive sulfide ore formation in an Iceland-style rift environment. Econ. Geol. Monograph 10, 471–498.
Prior, G.J., Gibson, H.L., Watkinson, D.H., Cousens, B.L., Cook, R., Barrie, T.C., 1999c. Sm-Nd isotope study of rhyolites from the Kidd Creek Mine area, Abitibi Subprovince, Canada. Econ. Geol. Monograph 10, 499–510.
Rogers, R., Ross, P.-S., Goutier, J., Mercier-Langevin, P., 2014. Using physical volcanology, chemical stratigraphy and pyrite geochemistry for VMS exploration: an example from the Blake River Group, Abitibi greenstone belt. Econ. Geol. 109, 61–88.
Ross, P.-S., McNicoll, V.J., Debreil, J.A., Carr, P., 2014. Precise U-Pb geochronology of the Matagami mining camp, Abitibi Greenstone Belt, Quebec: stratigraphic constraints

and implications for volcanogenic massive sulfide exploration. Econ. Geol. 109, 89–101.
Rutten, M.G., 1963. Acid lava flow structure (as compared to ignimbrites). Bull. Volcanol. 2, 111–121.
Schmid, H.-U., 1981. Descriptive nomenclature and classification of pyroclastic deposits and fragments: Recommendations of the IUGS Subcommission on the Systematics of Igneous Rocks. Geology 9, 41–43.
Shervais, J.W., 1982. Ti-V plots and the petrogenesis of modern and ophiolitic lavas. Earth Planet. Sci. Lett. 59, 101–118.
Spooner, E.T.C., Barrie, C.T., 1993. A special issue devoted to Abitibi ore deposits in a modern context: preface. Econ. Geol. 88, 1307–1323.
Sun, S.S., McDonough, W.F., 1989. Chemical and isotopic systematics of oceanic basalts; implications for mantle composition and processes. In: In: Saunders, A.D., Norry, M.J. (Eds.), Magmatism in the Ocean Basins 42. Geological Society Special Publications, pp. 313–345.
Thurston, P.C., Ayer, J.C., Goutier, J., Hamilton, M.A., 2008. Depositional Gaps in Abitibi Greenstone Belt Stratigraphy: a key to exploration for syngenetic mineralzation. Econ. Geol. 103, 1097–1134.
Wachendorf, H., 1973. The rhyolite flows of the Lebombos (SE Africa). Bull. Volcanol. 35, 515–529.
White, J.D.L., Houghton, B.F., 2006. Primary volcaniclastic rocks. Geology 34, 677–680.
Williams, H.R., 1990. Subprovince accretion tectonics in the south-central Superiorprovince. Can. J. Earth Sci. 27, 570–581.
Wood, D.A., 1980. The application of a Th-Hf-Ta diagram to problems of tectonomagmatic classification and to establishing the nature of crustal contamination of basaltic lavas of the British Tertiary Volcanic Province. Earth Planet. Sci. Lett. 50, 11–30.
Wyman, D., Bleeker, W., Kerrich, R., 1999. A 2.7 Ga komatiite, low Ti tholeiite, arc tholeiite transition, and inferred proto-arc geodynamic setting of the Kidd Creek deposit: evidence from precise trace element data. Econ. Geol. Monograph 10, 525–542.